Understanding Microhabitat Distribution at the Riverscape: Insights from Coupled Hydrodynamic and Bioenergetic Modeling

A Thesis
Presented in Partial Fulfillment of the Requirements for the
Degree of Master of Science
with a
Major in Environmental Science
in the
College of Graduate Studies
University of Idaho
by

Richard A. Carmichael

Major Professor: Daniele Tonina, Ph.D.
Committee Members: Eva Strand, Ph.D.; Rohan Benjankar, Ph.D.; Kevin See, Ph.D.
Department Administrator: J.D. Wulfhorst, Ph.D.

May 2019

Authorization to Submit Dissertation

This dissertation of Richard A. Carmichael, submitted for the degree of Master of Science with a Major in Environmental Science and titled "Understanding Microhabitat Distribution at the Riverscape: Insights from Coupled Hydrodynamic and Bioenergetic Modeling" has been reviewed in final form. Permission, as indicated by the signatures and dates below, is now granted to submit final copies to the College of Graduate Studies for approval.

Major Professor: _____ Date: _____
Daniele Tonina, Ph.D.

Committee Members: _____ Date: _____
Eva Strand, Ph.D.

_____ Date: _____
Rohan Benjankar, Ph.D.

_____ Date: _____
Kevin See, Ph.D.

Department Administrator: _____ Date: _____
J.D. Wulfhorst, Ph.D.

Abstract

Understanding and evaluating complex links between anthropogenic and natural processes has become an essential piece in freshwater conservation and management. Characterization and monitoring of streams worldwide has been difficult due to the complex nature of river systems and the organisms that inhabitant them. With recent advances in technology and modeling techniques, the scientific community has begun to improve characterization of processes governing freshwater streams and rivers. To further understanding and management of river systems, we present novel technological and modeling techniques to gain insights into said links and provide guidance related to freshwater and fisheries management where we apply these methods to the Lemhi River of Eastern Idaho. First, we processed and validated a new generation bathymetric light detection and ranging system known as the Experimental Advanced Airborne Research LiDAR-B (EAARL-B). This newly developed aerial system relies on the travel time of light energy pules to measure distance from the sensor which generates high resolution mapping (~1 point/m^2) of stream corridors, including the bathymetry, banks, and floodplains at watershed scales (100 km). Next, we used a validated, bare earth filtered, digital surface model supported by the EAARL-B system to develop a series of numerical flow models for the assessment of aquatic habitat as it relates to endangered Chinook salmon. Leveraging the spatially continuous modeled depth and velocities, we coupled flow hydraulics with publicly available empirical data including: Lemhi River Chinook salmon length and mass distributions, drifting macroinvertebrate rates, measured stream temperature, and representative measured discharges to develop a bioenergetics model to assess the impacts of water diversion, stream flow, morphological channel simplification, and stream temperature on juvenile Chinook salmon habitat suitability of the mainstem Lemhi River. We compared three distinct 1 km reaches with variable morphological complexity, a single thread confined channel, a multithread complex reach, and an engineered restoration reach to model juvenile Chinook salmon bioenergetic profitability for two critical time periods, late summer low flow (August) and late fall, fully undiverted, natural flow regime (October). We conclude that morphological complexity, specifically side and off-channel habitat, is essential for supporting juvenile Chinook salmon growth. As temperature begins to decrease in the fall, and mainstem discharges are increased due to water management, the morphologically complex reach provided the greatest amount of suitable habitat to sustain or promote growth for juvenile Chinook salmon.

Acknowledgements

Thank you to the University of Idaho Center for Ecohydraulics Research, specifically Dr. Daniele Tonina and Dr. Elowyn Yager for providing me with amazing academic and research opportunities in addition to a one of a kind education that went far and above my expectations. Also, thank you to Jody White and Chris Beasley for allowing me the opportunity to pursue a higher education and continuing to support my work. Thank you to Mr. Mike Edmundson and the Idaho Governor's Office of Species Conservation for providing valuable insight and direction, as well as funding for the project. Lastly, thank you to my committee members Dr. Rohan Benjankar, Dr. Eva Strand, and Dr. Kevin See, without your help and guidance this project would not have been possible.

Dedication

I would like to dedicate my work to my mother and father for instilling in me a passion for the outdoors, conservation, and science. Thank you for your guidance, encouragement, and love.

Table of Contents

Authorization to Submit Dissertation ii

Abstract iii

Acknowledgements iv

Dedication v

Table of Contents vi

List of Tables vii

List of Figures viii

Chapter 1: Bathymetric LiDAR Filtering and Validation: application of the Experimental Advanced Airborne Research LiDAR-B 1

- Abstract 1
- Introduction 1
- Methods and Materials 5
- Results 8
- Discussion 9
- Conclusion 11
- Literature Cited 12

Chapter 2: Some Like It Low: A Bioenergetic Evaluation of Habitat Quality for Juvenile Chinook Salmon in the Lemhi River, Idaho 25

- Abstract 25
- Introduction 25
- Methods and Materials 27
- Results 32
- Discussion 34
- Conclusion 36
- Literature Cited 37

List of Tables

Table 1-1. Adjustable parameters used in the ground determination of the raw, unfiltered point cloud. 21

Table 1-2. Displaying point to point analysis results of average error and RMSE for each unique reach within our study area for ground classification using LAS Tools only and LAS Tools plus QTM AGL. 22

Table 1-3. Reach specific results of the 1m by 1m comparison of the LiDAR supported DEM to the RTK ground survey supported DEM. 23

Table 1-4. Complete results of residual elevation errors when comparing the final 1m DEM to the extended RTK survey points. Depths are placed in 20cm bins and the ME, median, RMSE, and count for each depth bin are displayed. 24

List of Figures

Figure 1-1. Overview map of the Lemhi River bathymetric LiDAR study area including; drainage basin locator map, filtered 1m DEM extent supported by LiDAR, and location of control reaches for the study. Background imagery provided by ESRI online. 15
Figure 1-2. A map displaying the two high-resolution RTK reaches for Site One. Reaches are colored individually by elevation values, overlaid on NAIIP background imagery 16
Figure 1-3. A map displaying the high resolution RTK survey for control Site Two with road points included. Points are colored by elevation, overlaid on background NAIIP imagery. 17
Figure 1-4. Spatial extent of the extended in channel RTK survey, with a callout of in channel points overlaid on NAIIP imagery. 18
Figure 1-5. A flow chart illustrating the processing and filtering work flow of the EAARL-B LiDAR data collected for this study within the Lemhi River, ID, paired with a brief overview description of each step. 19
Figure 1-6. A frequency distribution of elevation residuals of the extended RTK ground survey and the LiDAR supported DEM..... 20
Figure 2-1. Map of the Lemhi watershed and spatial locations of each modeled reach; Complex, Restoration, and Straight. The inset shows the location of the Lemhi drainage within the state of Idaho, USA. The map is displayed over imagery from the National Agriculture Imagery Program, coordinates are in GCS North American 1983. 43
Figure 2-2. Maps of the wetted area of each modeled scenario/reach. A) Fully diverted Complex; B)Fully undiverted Complex; C) Fully diverted Straight; D) Undiverted Straight; E) Fully diverted Restoration Closed; F) Undiverted Restoration Closed; G) Fully diverted Restoration Open; H) Undiverted Restoration Open. 44
Figure 2-3. Daily average discharge (solid red line), along with its 75th percentile (gray line) and 25th percentile (black line) calculated from all available discharge measurements at the Lemhi at Cottom Lane Idaho Department of Water Resources gauging station just upstream of the study reaches. 45
Figure 2-4. Calculated fraction of suitable habitat, defined with modeled NEI values meeting or exceeding the required maintenance ration for a given fork length, drift abundance, and temperature. Results are grouped by reach/flow scenario and colored by modeled fork length of 65, 75, 88, and 102 mm, from left to right and dark to light gray, respectively. 46
Figure 2-5. Spatially distributed results of all modeled feeding locations that either met or exceeded the calculated maintenance ration (AE $\geq$ 1) for the corresponding temperature and 50th percentile fork length of measured Lemhi River Chinook Salmon. Displaying all modeled reaches: A) Fully diverted Complex; B) Fully undiverted Complex; C) Fully diverted Straight; D) Undiverted Straight;

E) Fully diverted Restoration Closed; F) Undiverted Restoration Closed; G) Fully diverted Restoration Open; H) Undiverted Restoration Open. 47
Figure 2-6. Histograms of AE, the ratio of NEI to maintenance ration, for both August and October modeled scenarios. The y-axis displays the fraction of habitat area that falls within each bin of AE. The bars are colored by the corresponding reach for the 50th percentile fork length. The dotted line marks a bin value of 1 or greater, which indicate feeding stations have met or exceeded the calculated maintenance ration. 48
Figure 2-7. Total amount of suitable habitat (AE ≥ 1) for the entire reach, its main channel, and off-channel areas for the 50th percentile fork lengths of Lemhi River juvenile Chinook. 49
Figure 2-8. Percent of off-channel habitat with AE ≥ 1 (left graph) and percent of off-channel contribution to the total suitable area of each individual study reach and scenario (right graph). 50
Figure 2-9. Total available suitable habitat for the late August alternative flow scenario (all other variables held constant) expressed in percent of total suitable habitat (left graph) and in area (m^2) for the diverted and undiverted flows. 51
Figure 2-10. Total available suitable area for late October alternative flow scenario expressed in percent (left graph) and in area (m^2) (right graph) for diverted and undiverted flow. 52

Chapter 1: Bathymetric LiDAR Filtering and Validation: application of the Experimental Advanced Airborne Research LiDAR-B

Abstract

Light detection and ranging (LiDAR) technology has emerged as a leading method in data acquisition to support the generation of high resolution seamless digital elevation models (DEMs). However, limited scientific literature is available on LiDAR processing, filtering of ground and non-ground points, and the validation of LiDAR processing capability compared to a high accuracy, high resolution Real Time Kinematic (RTK) ground survey, the current surveying golden standard. In this study we processed, filtered, and analyzed the performance of the Experimental Advanced Airborne Research LiDAR (EAARL-B) in a bathymetric environment of Idaho, USA to: (i) present a filtering technique for semi-automation of ground and non-ground determination of points using a widely available set of tools called *Las Tools*, (ii) assess the accuracy of the EAARL-B performance to continuously map topobathymetry and lastly (iii) assess the limitations of green wavelength, full waveform, bathymetric LiDAR and the impacts of variable depth on vertical accuracy of the LiDAR data in a small mountainous stream. Our results show that *Las Tools* can determine and separate bare earth features from returns generated by the water's surface, turbidity in the water column, and vegetation overhanging the stream channel to support DEM generation on the 1m scale. Further, EAARL-B can resolve bathymetry at the cm scale with an in-channel root meet square error of 13 cm. These results and methods provide a framework for future LiDAR collection and processing and encourage researchers to further the use of both terrestrial and bathymetric LiDAR systems.

Introduction

Generation of seamless, high resolution, watershed scale (100's kms) digital surface models (DSMs) is rapidly becoming an essential piece in describing and modeling characteristics and processes important to aquatic habitat (Benjankar et al., 2016; Lyon et al., 2015; McKean et al., 2009a, 2008). It has also shown promise in calculations of sediment transport (Mandlburger et al., 2011), has proven utility in flood risk analysis and prediction (Leskens et al., 2017), characterization of riparian vegetation (Montealegre et al., 2015), and broadened understanding of topographic change processes (Wyrick and Pasternack, 2016). Studies have also shown its promise in supporting numerical flow simulations (McKean et al., 2014), where the digital surface model (DSM) or digital elevation model (DEM) accuracy is the most important boundary in numerical modeling of stream hydraulics, e.g. depth, velocity and shear stress distributions (Conner and Tonina, 2014; Pasternack et al., 2006).

Further, Light Detection and Ranging (LiDAR) technology has proven useful for monitoring of pre- and post-restoration actions in riverine environments (Mandlburger et al., 2011; McKean et al., 2009a). LiDAR measures the travel time of light emitted from a source, to the ground, and back to the sensor to map 3-dimensional surfaces and has developed as the leading technology in high resolution terrain and bathymetric mapping over large scales (Lyon et al., 2015).

Traditional airborne LiDAR (sometimes called terrestrial LiDAR) operates in the near infrared spectrum, whereas bathymetric LiDAR operates in the green spectrum (McKean et al., 2014). Near infrared light energy is completely absorbed by water and is ineffective in mapping bathymetric surfaces such as submerged streambeds; however green spectrum LiDAR can penetrate water and allows for energy returns back to the airborne sensor (Fernandez-Diaz et al., 2014). With recent advancements in computing and sampling technologies, our ability to map the bathymetry of rivers at high resolution (>20 points/m^2) and high vertical accuracy (<10 cm) over hundreds of kms of streams and rivers is becoming a reality (Mandlburger et al., 2015, 2011).

Continuous mapping of rivers is necessary for management of inland waterways (Steinbacher et al., 2010). Moreover, our ability to accurately map the bathymetry of freshwater and saltwater systems has dramatically improved over the last decade (Fernandez-Diaz et al., 2014; Pan et al., 2015). The accuracy and utility of airborne bathymetric LiDAR has been widely studied and reported; from coastal and marine environments (Hilldale and Raff, 2008; Kinzel et al., 2013; Pan et al., 2015), to large rivers (Pan et al., 2015; Saylam et al., 2017), and small mountainous streams (McKean et al., 2014, 2009b); the reported accuracies are typically in the tens of centimeters. Despite the plethora of research on LiDAR validation and utility, very little has focused on the processing and filtering of bathymetric LiDAR data. More notably, even less information is available in vegetated mountainous stream environments. A need for a widely available semi-automated bathymetric LiDAR processing and filtering technique has arisen within the scientific community.

Modern day LiDAR data sets are generally processed and filtered using proprietary software created by the companies that also manufacture the systems collecting the data (Hug et al., 2004; Montealegre et al., 2015). Classification of ground and noise points is essential to the generation of high resolution DEMs and filtering to bare earth is the most crucial step in DEM generation (Meng et al., 2010). Ground filtering has also proven to be the most challenging task in processing bathymetric LiDAR data along hundreds of kms of a river network (Chen, 2001). There have been several studies outlining the process of data filtering, but limited research has been done on the quantitative assessment of those filtering methods in a vegetated, mountainous stream environment.

Analysis of seven filtering algorithms and evaluation of classification generated by the filtering to that of a hand filtered/classified dataset in a Mediterranean forest environment, found the best performance when using the Multiscale Curvature Classification (Evans and Hudak, 2007) for separating return points into ground and non-ground (Montealegre et al., 2015). The second best performing algorithm was *Las Tools* (http:// rapidlasso.com/lastools/), which leverages a method developed by Axelsson (1999). The author's concluded that each algorithm and processing technique had strengths and weaknesses and that no single algorithm worked perfectly for classifying points into ground and non-ground. They also found that obstructions like sprouted scrub, woody debris, stumps, and slopes greater than 15 degrees caused the most difficulty in point filtering and classification. Pan et al. (2015) went one step further and evaluated the performance of several full-waveform processing algorithms in the Colorado River, USA and the Snake River, USA. They compared the performance of a continuous wavelet transformation, Gaussian decomposition method, and empirical system response waveform decomposition to the bathymetry generated by an Acoustic Doppler Current Profiler (ADCP). The study concluded that processing full waveform returns, and a continuous wavelet transform outperformed all other full waveform processing algorithms in the study. They also concluded that environmental factors such as water turbidity and substrate albedo can have a substantial impact on processing of full waveform returns, also concluding that there is not a single-best processing algorithm for all situations.

McKean et al. (2014) processed full waveform bathymetric LiDAR returns using the Airborne LiDAR Processing System (ALPS) (Nagle and Wright, 2016) in a small mountainous stream of Idaho, USA. They reported on typical vertical errors found in the literature (eg. Hilldale and Raff 2008), but they did not compare their results to a high resolution (>1 pt/m^2), high accuracy (RTK-dGPS) ground survey, nor did they provide information on point filtering or classification of ground and non-ground returns. Fernandez-Diaz et al. (2014) furthered knowledge using a new single-wavelength LiDAR sensor to map bathymetry in a wide range of study areas from coastal environments in Florida to large fresh water environments in the Blue and Colorado Rivers, USA to assess the accuracy of the Optech Aquarius bathymetric LiDAR system. The discrete returns from the sensor were classified into bathymetry, water, and ground by first removing noise, second applying a modified morphological filter from Axelsson (1999), and then separating the land-water boundary either manually or with the aid of ancillary information, finally correcting for incidence angle created from light travel through the water column. The results generated point densities ranging from 1-4 points/m^2 and mapped depths ranging from 0.15 m to 12 m. However, the study did not compare the performance of the LiDAR system and filtering technique to a high resolution, high accuracy ground survey. Although the study was focused on the performance assessment of the

Aquarius system, the authors stressed the need for more research into filtering and processing of both discrete and full waveform LiDAR returns.

Some research has been conducted regarding the use and application of LiDAR filtering methods in a terrestrial environment; however, very limited research has been done in an aquatic environment using bathymetric LiDAR datasets. Even less information is available in the scientific literature outlining workflow, processing, classification, and filtering of raw point clouds from green spectrum LiDAR sensors, most notably when commercial software from the manufacturer is unavailable. We address this knowledge gap and focus on how to handle large bathymetric point cloud datasets, as well as classifying point clouds into ground and non-ground.

We propose a workflow and filtering algorithm to help facilitate point cloud filtering and classification that may be applicable to a wide range of LiDAR sensors and raw point cloud datasets. Because much of the current scientific literature has investigated point cloud filtering in canopy height models, terrestrial LiDAR datasets, and full waveform bathymetric LiDAR processing, we suggest a workflow that simply classifies bathymetric and terrestrial points into ground and non-ground to support the generation of a high resolution (1 m grid) DSMs. We apply this method to LiDAR data collected in a small mountainous stream environment, the Lemhi River (Central Idaho, USA). We use the raw point cloud collected by the Experimental Advanced Airborne Research LiDAR-B (EAARL-B) to investigate the accuracy of point classification into ground and non-ground points using a widely available set of tools called *LAS Tools* (http:// rapidlasso.com/lastools/). We further filter the dataset and finalize the DEM(s) generation using a set of tools developed *by Applied Imagery* called *Quick Terrain Modeler (QTM)*. We propose a workflow and set algorithm parameters that best filter a raw point cloud and compare the results to two distinct study reaches with areas of extreme amounts of vegetation, to not only test the limits of the green wavelength bathymetric LiDAR EAARL-B system, but to also test the limits of LiDAR filtering and classification as a function of water depth within the channel. We then compare the filtered point cloud and DEM supported by the EAARL-B to multiple high-resolution ground surveys (1.6 point/m^2) collected by a field crew using a high accuracy real time kinematic digital GPS device (RTK-dGPS) in two morphologically distinct study reaches. We further evaluate the final DEM supported by the LiDAR with a DEM to DEM comparison of the LiDAR supported surface model to the ground RTK supported surface model. Unique to this study, we extend our validation with a spatially distributed collection of 454 in-channel RTK ground points covering roughly the upper 25 river kms of the study reach by comparing the elevation of those points to our final 1 m DEM supported by the filtered LiDAR. Finally, we discuss limitations of point filtering based on vertical error as a function of water

depth and present ideas for future filtering and classification of bathymetric LiDAR point clouds for potential users of LiDAR data across all types of environments.

Methods and Materials

Study Site

The study was conducted in the Lemhi River of Eastern Idaho, USA. The average bankfull width of the reach ranges from <4 to >20 meters, with very large amounts of overhanging vegetation as well as canopy cover from mature Cottonwood (*Populus* spp.) and Willow (*Salix* spp.) species. Two morphologically distinct sites were selected to evaluate the performance of the EAARL-B and LiDAR filtering by comparing results to high-resolution RTK-dGPS ground surveys (Figure 1-1).

The upstream study site (Site One) was sampled as two separate reaches; Site One Reach One is located just upstream of Site One Reach Two, with a length of 165 m, consisting of pool, riffle, bar, and run habitat types. Site One Reach Two is a 240 m long meandering stretch, consisting of pool-riffle sequences like Site One Reach One (Figure 1-2). Both reaches have an average width of 10 m with substrate ranging from sand and fines (<2 mm) to cobble (64 mm).

The furthest downstream site (Site Two) was comprised of a straight, uniform, plane-bed morphology type (Figure 1-3) with a median grain sizes ranging from sand and fines (<2 mm) to cobbles (64 mm). The site is confined by a paralleling highway for the entirety of its length.

Both reaches had variable amounts of overhanging vegetation and riparian cover along the banks. The RTK validation points also covered areas of the highway paralleling the study reach, in addition to RTK points spread throughout the upper 25 kms of the study area (Figure 1-4).

An attempt was made to collect points spread evenly throughout the 25 km; however, entree to the channel was limited in some locations by velocity and depth. Access to the point collection locations for the upper 25 km extended RTK survey was made possible by a small inflatable cataraft.

Data Collection

A ground crew collected high resolution RTK-dGPS surveys in both Site One and Site Two reaches with a point density of 1.6 points per m^2 in the channel. Points were also collected on top of the highway surface paralleling the river roughly every 1 km for nearly 30 kms. High resolution RTK-dGPS points were collected in channel opportunistically, totaling 454 additional validation points (Figure 1-4). The in-stream depth at the RTK validation points was also collected to further asses the impacts of stream depth on the error of the LiDAR.

The topobathymetric LiDAR dataset was acquired using the EAARL-B (Wright et al., 2016), the latest generation of EAARL systems originally developed by National Aeronautical Space Agency (NASA) and the United States Geological Survey (USGS) (McKean et al., 2014, 2009b). Three days of flight were conducted, and multiple passes were flown focusing on in-channel and flood plain habitat to increase return density within the stream corridor. The unit operates at a flying altitude of 300 m, with a scan rate of 25 Hz, and an illumination spot diameter (or beam divergence) of 15-20 cm, capable of omitting 30,000 pulses/s. Full waveform returns are digitized on board and discrete returns are recorded by the sensor. An on-board inertial measurement unit (IMU) tracks the relative position of the sensor, and collects real time measurements of roll, pitch, and yaw.

Data Processing and Filtering

The ALPS was used to process continuous full waveform returns to the onboard digitizer (Nagle and Wright, 2016). The software was also used to account for the change in travel speed of light at the air to water interface as well as apply any roll, pitch or yaw bias that may have been recorded by the IMU during data collection. Three days of flight were conducted, and average calculated biases created by aircraft roll, pitch, and yaw were applied based on each day of flight. The ALPS software package was used to interpret the onboard digitized full waveform returns in order to produce 3-dimensional point returns (x,y,z) leveraging the standard bathymetry algorithm (Nagle and Wright, 2016). The processing yielded an extremely dense and robust dataset at just over 2 points/m² (after the noise removal process), but the point cloud still included returns borne from the water's surface, water column, and vegetation, in addition to a small amount of returns below the surface of the earth. Further filtering to designate ground and non-ground points was still necessary.

The first step in filtering the raw point cloud was to tile the dataset. The act of tiling divides the point cloud into manageable sections based on a certain length and width (or step x,y) of the tiles. This allows the user to reduce the number of data points selected by the chosen tile size and in turn reduce computational requirements. It also allows *LAS Tools* to function more efficiently (Hug et al., 2004). It is important to understand the density of the point cloud to ensure that tiles are of adequate size. Tiles can be remerged for future visualization and analysis of the entire point cloud. Our dataset was tiled using a function of *LAS Tools* called *Las Tile*, with a step size of 1000 m by 1000 m.

The second step to filtering and classifying the point cloud was to remove any noise from the dataset. The user must filter out noise points that may arise from returns borne by backscatter, or energy reflected from objects other than bare earth, such as power lines, water surface, water turbidity, birds, diversions, etc. An important consideration when using the *LAS Tools* function *LAS Noise* for noise removal of your data is the step size in both the x and y direction, but also the step size in the vertical

or z direction. The step values we used were 2 m in both the x and y direction and ±0.1 m in the vertical direction or z step. These parameters determine a 3-dimensional box or search radius around each individual point, to evaluate the number of other points that fall within that given search area or box (point isolation analysis). The user defines a threshold value of the number of other returns that must fall within that search area to determine if the point should be classified as noise and thus be removed from the dataset. The goal of noise filtering should be to remove as many erroneous returns as possible while maintaining point density below thick vegetation at the bare earth elevation. Areas of interest when visually assessing the noise filtering algorithm should be focused near the stream banks, where considerable amounts of vegetation may be present, reducing the number of returns to the ground. Also, if any road surfaces are available within the datasets domain, the user can qualitatively assess performance of noise removal by visually analyzing cross sections along road surfaces to ensure no points are extending below the roads elevation. After visual assessment of the noise removal process, best results for our data were yielded when the threshold value was set at 6 points.

The third and most critical step in filtering our bathymetric point cloud was the utilization of the *Las Tools* function *Las Ground New*. We iteratively tested and adjusted the parameters of the tool (Table 1-1) on a test reach of the sampled area to produce a ground and non-ground classified point cloud that: 1) captured steep inflections along the bank and in channel, most notably near transitions from pools to riffles, 2) produced a smooth bed form in accordance with what was visually analyzed during ground surveys, and 3) maintained relatively high point densities in channel (1 point/m^2). We then applied the same settings to the entirety of the previously tiled and noise removed dataset.

The final point cloud filtering results from *LAS Tools* were further filtered using *Quick Terrain Modeler*'s (QTM) *Above Ground Level Analysis* (AGL) tool (Varela-González et al., 2013). The tool generates an initial ground level estimate from the provided point cloud, the user can then trim/filter points based on elevation relative to the initial ground level estimate. The initial ground estimate was generated on a 1 m by 1 m grid, and the point cloud was cropped at 0.1 m above the ground estimate and 0.1 m below the elevation of the ground estimate. Thus, any points that fell outside of +-0.1 m from the ground estimate were excluded from the point cloud.

Accuracy Analysis

Vertical accuracy of the filtered LiDAR point cloud was analyzed by comparing point by point elevations to ground control RTK surveys. We compared filtered LiDAR points using *Las Tools* only

and the further filtered QTM AGL points to those of two high-resolution ground surveys within our two morphologically distinct control sites. A 10 cm radius was drawn around each RTK point and the difference between the RTK point elevation and the average elevation of the ground designated LiDAR points falling within that radius was calculated. The 10 cm radius was selected because this is the radius of the LiDAR laser footprint. Also, a DEM to DEM elevation comparison was conducted by subtracting the two 1 m DEMs supported by the LiDAR data filtered with *LAS Tools* only and the *LAS Tools* plus *QTM AGL* filtering to that supported by the field data within the study reaches. For both analyses (point-to-point and DEM-to DEM) and both filtering techniques, we calculated the mean error (*ME*) or bias and the root mean square error (*RMSE*),

$$ME = \frac{\sum_{i=1}^{n} \left(y_i^g - y_i^l \right)}{n} \tag{1}$$

$$RMSE = \sqrt{\frac{\sum_{i=1}^{n} \left(y_i^g - y_i^l \right)^2}{n}} \tag{2}$$

where y_g and y_l are the elevations of the ground and LiDAR surveyed points respectively and n the total number of points. Because the *RMSE* contains two kinds of errors: a systematic error due to difference between the mean elevations of the points, which is a bias (*ME*), and precision, we report both values.

To further test and validate the LiDAR supported final 1 m DEM and filtering performance for a much longer stream section of the study reach, we compared DEM elevation values at the 454 locations collected with RTK along the uppermost 25 km of the river. Because this paper is focused on bathymetric LiDAR filtering, we will only report on in-channel results from the study.

Results

Point to Point Comparison

An in-channel *RMSE* of 13 cm was calculated for the three study reaches for each filtering method (Table 1-2). Our results are well within average values reported in the literature for bathymetric LiDAR error (Fernandez-Diaz et al., 2014; Hilldale and Raff, 2008; McKean et al., 2014).

DEM to DEM Comparison

An in-channel *RMSE* of 11 cm was calculated when comparing the 1 m DEM supported by LiDAR and filtered with *Las Tools* only to the 1 m DEM supported by the RTK ground. An in-channel *ME* of 9 cm was calculated when filtering with *Las Tools* only. Within each individual study reach the *RMSE* and average absolute error stayed constant or increased (Table 1-3).

Extended RTK Point to DEM Comparison

Comparison between the elevations of our extended in-channel RTK survey points to the elevation of the final 1m DEM supported by the LiDAR and *LAS Tools* only filtering has a *ME* of -0.047 m and *RMSE* of 0.15 m (Figure 1-5). Unlike previous findings (Fernandez-Diaz et al., 2014; McKean et al., 2014) performed at reach scale, errors in the final 1 m DEM compared to the extended RTK survey show *RMSE* decreases with increasing depth, but then increases as the depth goes above 1 m (Table 1-3). The lowest *RMSE* occurs at a depth range of 0.8 m to 1 m with the greatest error being calculated at depths less than 0.2 m. A histogram of the elevation residuals (Figure 1-6) shows that most values fall between +-0.2 m, with two outlying errors of -0.84 m and -0.63 m respectively. When comparing the overall measured to modeled values of the extended ground survey we calculated an R^2 value of 1.

Discussion

In this study, we evaluated the accuracy of the EAARL-B system to what is widely considered the current golden standard in surveying accuracy, RTK-dGPS. Overall, we found that the in-channel RMSE of the LiDAR data was 13 cm. Limitations not only in data collection, but also in data filtering were present when unfiltered and filtered point clouds were visually compared, most noticeably in areas where the channel was relatively narrow. The EAARL-B penetrated vegetation and the water column, but the number of returns from the bedform was extremely limited. This caused the *Las Ground New* algorithm to interpret areas above the stream bed as "ground" where return density was much higher, instead of the lowermost points, which appeared to be returning from bare earth. The instrument struggled to resolve bathymetry in areas with high amounts of debris and large boulders that limited returns to the instrument from the lowermost bedform elevations. These areas include localized boulders, debris, and/or large plastic tarps, which were built up to create an in-channel obstruction to divert water from the main channel to irrigation diversions. Furthermore, in areas where the water was extremely shallow (<20 cm), it appears the filtering algorithm was interpreting the water's surface as ground instead of the bathymetry of the channel. This is most likely attributed to a limitation of the instrument itself, a result of the pulse width of 1 ns, which results in a pulse length of 15 cm of travel in air and thus masking the location of surface water and bottom elevations.

The LiDAR data collection and filtering performed best at a water depth of 0.8 m to 1.0 m. This seems to be the ideal depth for maximization of performance, whereas the *RMSE* increases at depths greater than 1 m. However, the limited number of points for water depths deeper than 1 m, only six, may bias this result. Furthermore, the deepest areas of the channel are quite small and narrow and typically surrounded by overhanging vegetation, as these are forced pools forming at the outside of

bends near vertical banks in the Lemhi. These three aspects, overhanging vegetation, small areal extent confined by steep banks, highly decrease the performance of the filtering algorithms. Thus, lower performance of the instrument and filtering within our study domain is lower in the deepest portions of the channel maybe be due to several reasons and may not directly depend on water depth. In streams where, deep water may extend over large areas, the error may not increase, and it should be tested.

When RTK points were compared to EAARL-B generated DEM in the extended in-channel survey, the average error was negative, which may suggest that the filtering algorithm did not completely resolve the bathymetry within pools in several locations. This may be another case where the number of returns from deep pools were so limited that either the noise removal process trimmed those as such, or the ground algorithm was unable to discern those from points within the water column just above to those at the actual ground elevation. Also, the *RMSE* of the extended RTK point to DEM comparison was 2 cm higher than that of the point to point comparison within our control reaches. This may be attributed to interpolation error of the DEM generation, but it may also be a function of timing of sampling. The original ground control surveys and LiDAR data collection occurred in the fall of 2013 but the extended RTK survey occurred in the fall of 2016. It is possible that in those three years the channel may have changed throughout the reach, creating more error in the extended RTK point to final LiDAR supported DEM comparison. Lastly, most elevation residuals from the extended survey were within ±0.2 m; however, two outliers of -0.84 and -0.63 were present. The residual value of -0.84 m occurred in an area of the channel with a deep pool, surrounded by sharp inflections. This was also a location where overhanging vegetation covered nearly the entire lateral extent of the channel where the RTK point was taken. This combination of factors leads to an extreme overestimate of elevation by the LiDAR supported DEM. The residual value of -0.63 m was calculated at a location of a small, deep, pool confined to one side of the channel. This is most likely a location where the RTK point was taken at the head of the pool, near the steep inflection, thus creating an error in the LiDAR generated DEM.

An attempt to further filter noise from the ground classified point cloud was also investigated, as indicated in the methods and results section. *Applied Imagery's Quick Terrain Modeler* and *Above Ground Level Analyst* was coupled with *LAS Tools* to reduce noise and remove points that may have been erroneously classified as "ground" in the original filtering. The results from the combination of the two toolkits *LAS Tools* and then *QTM* resulted in a lower bank, floodplain, and road *RMSE* compared to *LAS Tools* only, but the results for in channel *RMSE* were not affected, at 13 cm for both methods. Furthermore, the reduction in point density from the increased filtering resulted in a higher

in channel *RMSE* for the 1-m DEM comparison when supported by the combination of *LAS Tools* and *QTM AGL* Analysis, where an *RMSE* of 11 cm for *LAS Tools* only was reported and an *RMSE* of 12 cm for the combination of the two methods was calculated. In addition, each specific reach either stayed constant in the calculated *RMSE* value or increased slightly in *ME* with the further filtering. This is important because it highlights the difficulty in filtering to ground only. Increased filtering/point reduction may lead to less scatter in the ground designated points; however, it may also lead to higher error in the resulting DEM due to a reduction in point density and an increase in interpolation distances between points (Guo et al., 2010).

Conclusion

The point by point comparison revealed adequate data collection and ground designation when comparing the LiDAR supported point cloud to that of the ground survey. Results indicated that the EAARL-B and *Las Tools* combine to resolve bathymetry at the 10's of cm scale, but are limited at the micro-habitat (cobble scale), similar to findings from other studies (Hilldale and Raff, 2008). The instrument can penetrate dense vegetation near the banks, though these areas resulted in a higher *RMSE* than in-channel or flood plain returns, those outcomes are beyond the scope of this study and where investigated elsewhere (Tonina et al., 2018) . These results could be attributed to not only the dense vegetation reducing the number of points to the ground, but also sharp inflections in the banks where the instrument struggles to resolve the topography (McKean et al., 2014).

The 25 km in channel RTK validation of the final 1 m DEM was the first time to our knowledge that any bathymetric LiDAR supported DEM had been validated at that extended scale. The results were extremely promising and well within other reported values in the literature. This may provide confidence and reassurance to prospective users of remote sensing technologies that the products produced (DEM, DSM) are well tested and validated for use in management and application purposes. This may also open the door to more advanced and extended validation techniques of future data collection and analysis.

More broad implications of these results demonstrate not only the accuracy of current bathymetric LiDAR technology, but also highlight the applicability and utility of *LAS Tools* to filter massive datasets where water surface, vegetation, and other noise returns exist. Prospective users of bathymetric LiDAR data now have a framework available for the processing and filtering of point cloud data. Furthermore, this process and filtering technique may help to improve ground determination in raw point clouds that have already been sampled and analyzed in previous studies. The EAARL-B and proposed filtering technique combined to resolve the bathymetry at the 10's of cm scale, but the techniques are inadequate to map at the micro habitat or cobble scale. Increased

point density, reduction in pulse width (in conjunction with a reduction in pulse energy to maintain eye safety), better water surface identification techniques, and improved DEM generation algorithms may all be appropriate avenues for more research and further development of airborne bathymetric LiDAR sensors. Combinations of technological and computational advances may eventually lead to basin wide mapping at the grain scale as opposed to current methods limited to the channel unit scale.

Literature Cited

Axelsson, P., 1999. Processing of laser scanner data - Algorithms and applications. ISPRS J. Photogramm. Remote Sens. 54, 138–147. https://doi.org/10.1016/S0924-2716(99)00008-8

Benjankar, R., Tonina, D., Marzadri, A., McKean, J., Isaak, D.J., 2016. Effects of habitat quality and ambient hyporheic flows on salmon spawning site selection. J. Geophys. Res. G Biogeosciences 121, 1222–1235. https://doi.org/10.1002/2015JG003079

Chen, Q., 2001. PHOTOGRAMMETRIC ENGINEERING & REMOTE SENSING Airborne Lidar Data Processing and Information Extraction 109–112.

Conner, J.T., Tonina, D., 2014. Effect of cross-section interpolated bathymetry on 2D hydrodynamic model results in a large river. Earth Surf. Process. Landforms 39, 463–475. https://doi.org/10.1002/esp.3458

Evans, J.S., Hudak, A.T., 2007. A Multiscale Curvature Algorithm for Classifying Discrete Return LiDAR in Forested Environments. Ieee Trans. Geosci. Remote Sens. 45, 1029–1038. https://doi.org/10.1109/TGRS.2006.890412

Fernandez-Diaz, J.C., Glennie, C.L., Carter, W.E., Shrestha, R.L., Sartori, M.P., Singhania, A., Legleiter, C.J., Overstreet, B.T., 2014. Early results of simultaneous terrain and shallow water bathymetry mapping using a single-wavelength airborne LiDAR sensor. IEEE J. Sel. Top. Appl. Earth Obs. Remote Sens. 7, 623–635. https://doi.org/10.1109/JSTARS.2013.2265255

Guo, Q., Li, W., Yu, H., Alvarez, O., 2010. Effects of Topographic Variability and Lidar Sampling Density on Several DEM Interpolation Methods. Photogramm. Eng. Remote Sens. 76, 701–712. https://doi.org/10.14358/PERS.76.6.701

Hilldale, R.C., Raff, D., 2008. Assessing the ability of airborne LiDAR to map river bathymetry. Earth Surf. Process. Landforms 33, 773–783. https://doi.org/10.1002/esp.1575

Hug, C., Krzystek, P., Fuchs, W., 2004. Advanced lidar data processing with LasTools. XXth ISPRS

Congr. 12–23.

Kinzel, P.J., Legleiter, C.J., Nelson, J.M., 2013. Mapping River Bathymetry With a Small Footprint Green LiDAR: Applications and Challenges. J. Am. Water Resour. Assoc. 49, 183–204. https://doi.org/10.1111/jawr.12008

Leskens, J.G., Kehl, C., Tutenel, T., Kol, T., Haan, G. de, Stelling, G., Eisemann, E., 2017. An interactive simulation and visualization tool for flood analysis usable for practitioners. Mitig. Adapt. Strateg. Glob. Chang. 22, 307–324. https://doi.org/10.1007/s11027-015-9651-2

Lyon, S.W., Nathanson, M., Lam, N., Dahlke, H.E., Rutzinger, M., Kean, J.W., Laudon, H., 2015. Can low-resolution airborne laser scanning data be used to model stream rating curves? Water (Switzerland) 7, 1324–1339. https://doi.org/10.3390/w7041324

Mandlburger, G., Hauer, C., Wieser, M., Pfeifer, N., 2015. Topo-bathymetric LiDAR for monitoring river morphodynamics and instream habitats-A case study at the Pielach River. Remote Sens. 7, 6160–6195. https://doi.org/10.3390/rs70506160

Mandlburger, G., Pfennigbauer, M., Steinbacher, F., Pfeifer, N., 2011. Airborne hydrographic LiDAR mapping - Potential of a new technique for capturing shallow water bodies. 19th Int. Congr. Model. Simul. - Sustain. Our Futur. Underst. Living with Uncertainty, MODSIM2011, December 12, 2011 - December 16 2416–2422.

McKean, J., Isaak, D., Wright, W., 2009a. Chapter 2.—Stream and Riparian Habitat Analysis and Monitoring with a High-Resolution Terrestrial-Aquatic LiDAR. PNAMP Spec. Publ. Remote Sens. Appl. Aquat. Resour. Monit. 7–16.

McKean, J., Isaak, D., Wright, W., 2009b. Improving stream studies with a small-footprint green lidar. Eos (Washington. DC). 90, 341–342. https://doi.org/10.1029/2009EO390002

McKean, J., Tonina, D., Bohn, C., Wright, C.W., 2014. Effects of bathymetric lidar errors on flow properties predicted with a multi-dimensional hydraulic model. J. Geophys. Res. Earth Surf. 119, 644–664. https://doi.org/10.1002/2013JF002897

McKean, J.A., Isaak, D.J., Wright, C.W., 2008. Geomorphic controls on salmon nesting patterns described by a new, narrow-beam terrestrial-aquatic lidar. Front. Ecol. Environ. 6, 125–130. https://doi.org/10.1890/070109

Meng, X., Currit, N., Zhao, K., 2010. Ground filtering algorithms for airborne LiDAR data: A review of critical issues. Remote Sens. 2, 833–860. https://doi.org/10.3390/rs2030833

Montealegre, A.L., Lamelas, M.T., De La Riva, J., 2015. A Comparison of Open-Source LiDAR Filtering Algorithms in a Mediterranean Forest Environment. IEEE J. Sel. Top. Appl. Earth Obs. Remote Sens. 8, 4072–4085. https://doi.org/10.1109/JSTARS.2015.2436974

Nagle, D.B., Wright, C.W., 2016. Algorithms used in the Airborne LiDAR Processing System (ALPS) 46.

Pan, Z., Glennie, C., Hartzell, P., Fernandez-Diaz, J.C., Legleiter, C., Overstreet, B., 2015. Performance assessment of high resolution airborne full waveform LiDAR for shallow river bathymetry. Remote Sens. 7, 5133–5159. https://doi.org/10.3390/rs70505133

Pasternack, G.B., Gilbert, A.T., Wheaton, J.M., Buckland, E.M., 2006. Error propagation for velocity and shear stress prediction using 2D models for environmental management. J. Hydrol. 328, 227–241. https://doi.org/10.1016/j.jhydrol.2005.12.003

Saylam, K., Hupp, J.R., Averett, A.R., John, A., Jackson, K.G., Saylam, K., 2017. Quantifying the Bathymetry of the Lower Colorado River Basin, Arizona, with Airborne LiDAR.

Steinbacher, F., Pfennigbauer, M., Ullrich, A., Aufleger, M., 2010. Airborne hydromapping area-wide surveying of shallow water areas. Wasserwirtschaft 99, 10–14.

Tonina, D., McKean, J.A., Benjankar, R.M., Wright, W., Goode, J.R., Chen, Q., Reeder, W.J., Carmichael, R.A., Edmondson, M.R., 2018. Mapping river bathymetries: evaluating topobathymetric LiDAR survey. Earth Surf. Process. Landforms. https://doi.org/10.1002/esp.4513

Varela-González, M., González-Jorge, H., Riveiro, B., Arias, P., 2013. Performance testing of LiDAR exploitation software. Comput. Geosci. 54, 122–129. https://doi.org/10.1016/j.cageo.2012.12.001

Wyrick, J.R., Pasternack, G.B., 2016. Revealing the natural complexity of topographic change processes through repeat surveys and decision-tree classification. Earth Surf. Process. Landforms 41, 723–737. https://doi.org/10.1002/esp.

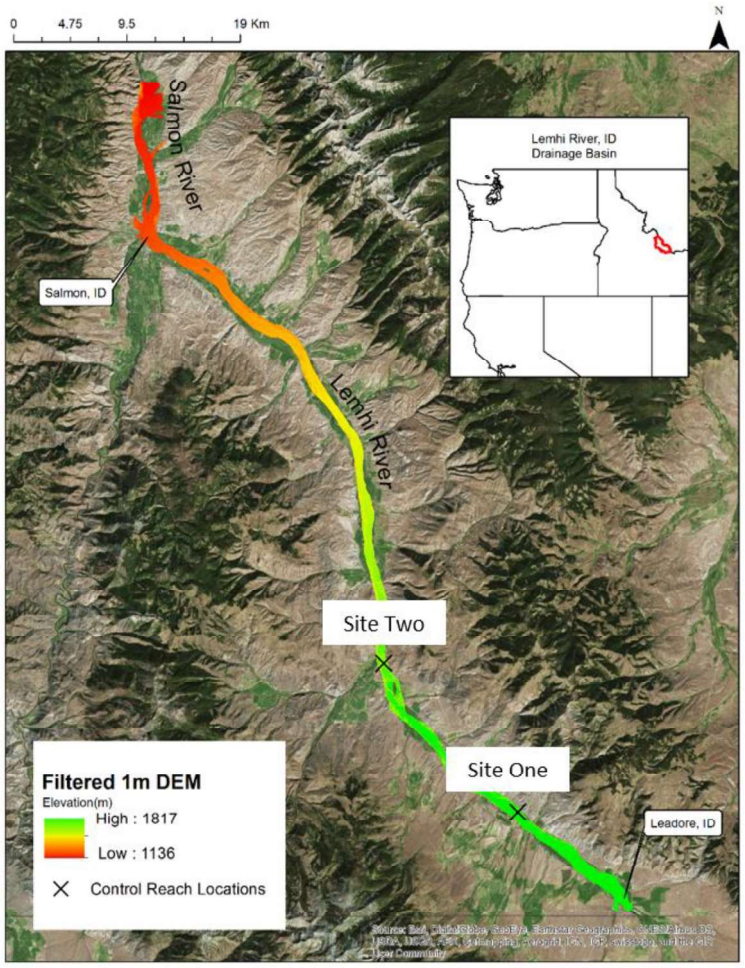

Figure 1-1. Overview map of the Lemhi River bathymetric LiDAR study area including; drainage basin locator map, filtered 1m DEM extent supported by LiDAR, and location of control reaches for the study. Background imagery provided by ESRI online.

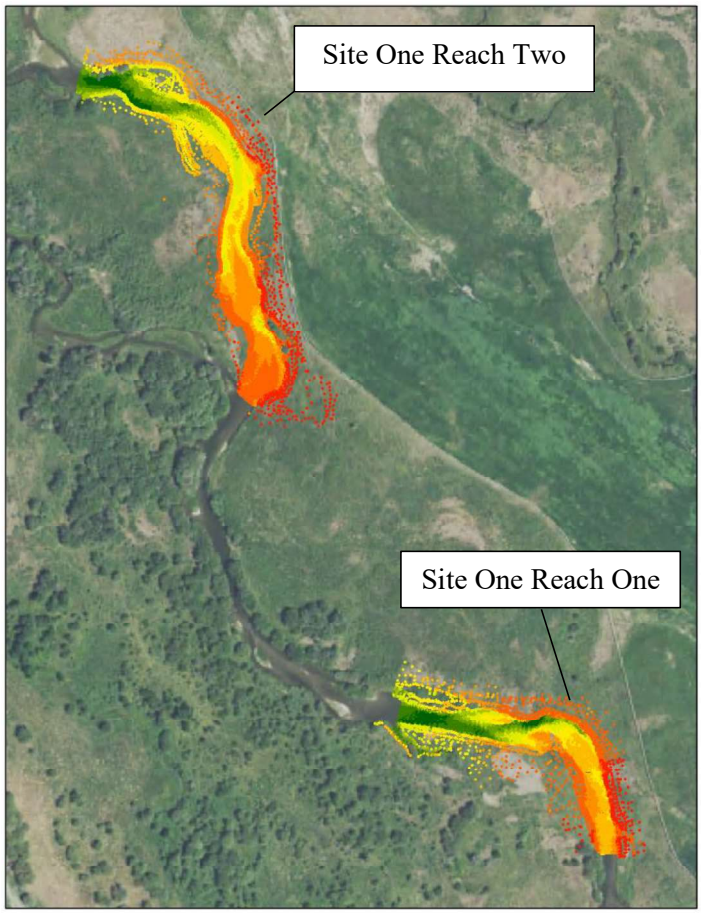

Figure 1-2. A map displaying the two high-resolution RTK reaches for Site One. Reaches are colored individually by elevation values, overlaid on NAIIP background imagery.

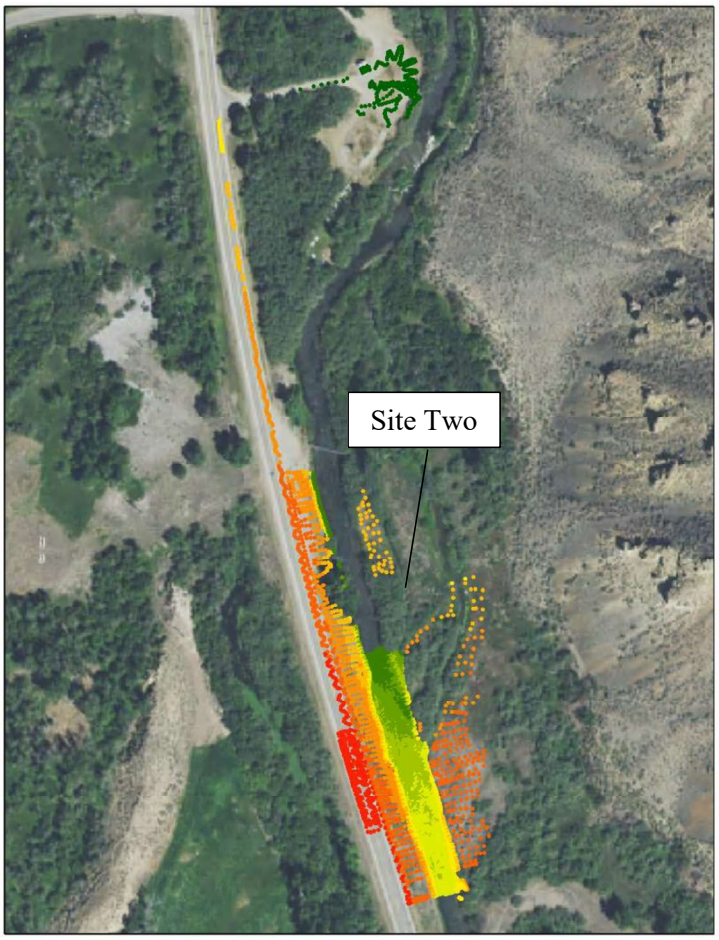

Figure 1-3. A map displaying the high resolution RTK survey for control Site Two with road points included. Points are colored by elevation, overlaid on background NAIIP imagery.

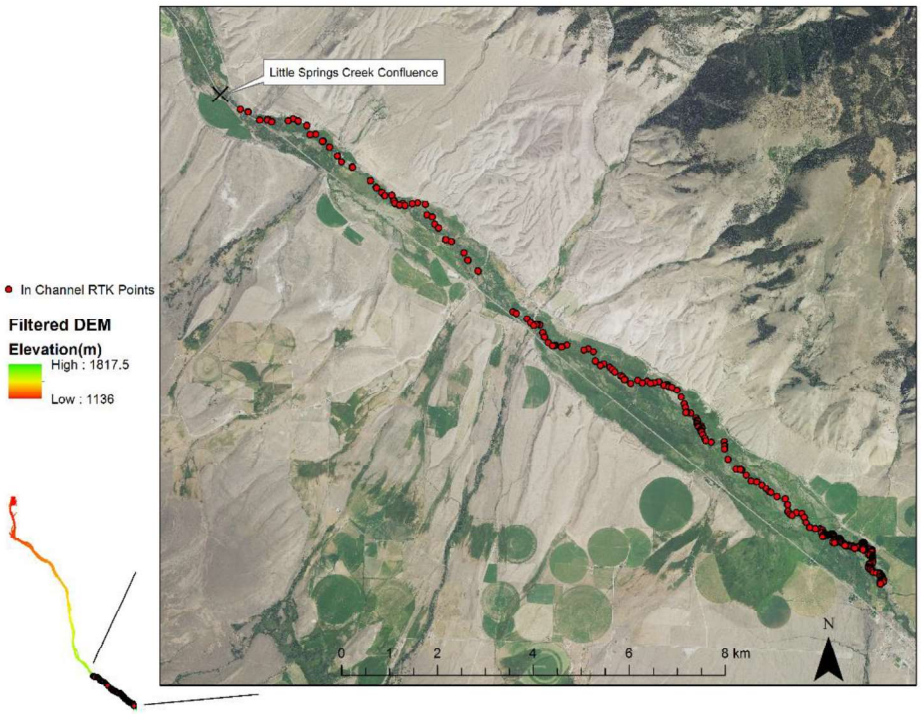

Figure 1-4. Spatial extent of the extended in channel RTK survey, with a callout of in channel points overlaid on NAIIP imagery.

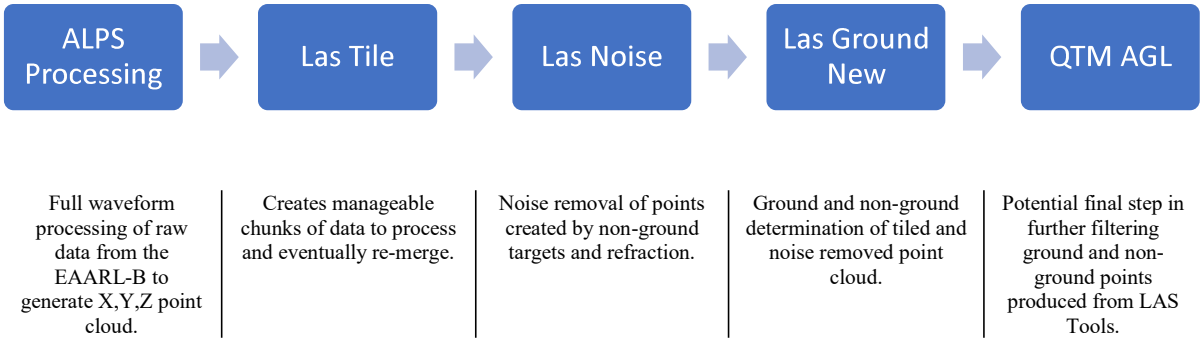

Figure 1-5. A flow chart illustrating the processing and filtering work flow of the EAARL-B LiDAR data collected for this study within the Lemhi River, ID, paired with a brief overview description of each step.

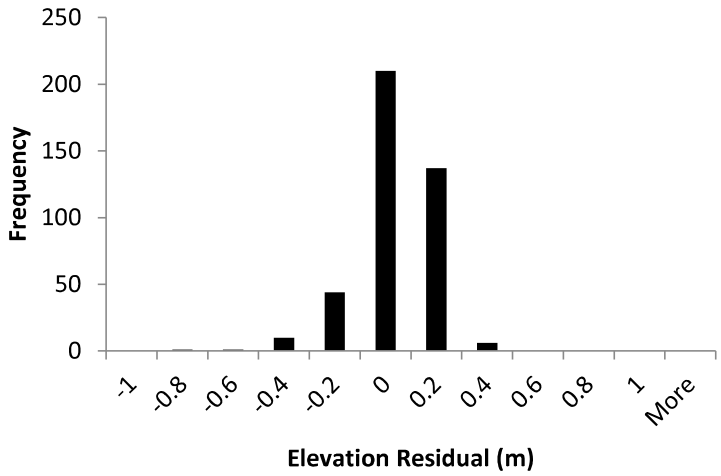

Figure 1-6. A frequency distribution of elevation residuals of the extended RTK ground survey and the LiDAR supported DEM.

Table 1-1. Adjustable parameters used in the ground determination of the raw, unfiltered point cloud.

Parameter	Value	Description/Notes
Step Size (m)	2	The length and width of the grid cell size placed across the dataset to search for ground points.
Search Parameter	'Hyper Fine'	Initial ground point definition/determination
Bulge (m)	0.0001	Regulates the distance that the initial ground estimate can bulge upward to incorporate other points within the dataset.
Upspike (m)	0.01	Helps remove any water surface points or water column returns (spikes) from the initial dataset; however, if the upspike removal is set too fine the user may start to see the removal of in-channel islands and bars.
Downspike (m)	0.2	Like issues previously highlighted with the upspike removal, if this parameter is set too fine the user may start to see the bottom of deep pools being designated as non-ground and removed from the dataset.
Offset (m)	0.0001	This parameter determines the vertical distance that the ground estimate can re-sample the original input point cloud to include those points in the final ground designation/determination.

Table 1-2. Displaying point to point analysis results of average error and RMSE for each unique reach within our study area for ground classification using LAS Tools only and LAS Tools plus QTM AGL.

Channel	LAS Tools Only		LAS Tools Plus QTM	
	ME (m)	RMSE (m)	ME (m)	RMSE (m)
S1R1 Channel	0.10	0.13	0.11	0.13
S1R2 Channel	0.13	0.15	0.13	0.15
S2 Channel	0.10	0.13	0.09	0.11

Table 1-3. Reach specific results of the 1m by 1m comparison of the LiDAR supported DEM to the RTK ground survey supported DEM.

Channel	LAS Tools Only		LAS Tools Plus QTM	
	ME (m)	RMSE (m)	ME (m)	RMSE (m)
S1R1 Channel	0.12	0.13	0.12	0.14
S1R2 Channel	0.08	0.10	0.09	0.11
S2 Channel	0.08	0.10	0.08	0.10

Table 1-4. Complete results of residual elevation errors when comparing the final 1m DEM to the extended RTK survey points. Depths are placed in 20cm bins and the ME, median, RMSE, and count for each depth bin are displayed.

Depth Range (m)	ME	Median	RMSE	Count
<0.2	0.149	-0.120	0.208	27
0.2-0.4	0.102	-0.077	0.173	154
0.4-0.6	0.046	-0.025	0.143	135
0.6-0.8	0.002	0.033	0.134	58
0.8-1.0	0.046	0.056	0.105	23
>1.0	0.104	0.087	0.158	6

Chapter 2: Some Like It Low: A Bioenergetic Evaluation of Habitat Quality for Juvenile Chinook Salmon in the Lemhi River, Idaho

Abstract

Management and conservation of freshwater habitat requires fine spatial resolution, watershed-scale, and life stage specific methods due to complex linkages among land, climate, water uses, and aquatic organism requirements. In this study, we present a valley-scale micro-habitat resolution, process-based bioenergetics approach that combines high-resolution topobathymetric LiDAR survey with two-dimensional hydrodynamic and bioenergetics modeling. We applied the model to investigate the role of lateral habitat, stream morphological complexity, water use, and temperature regimes on aquatic habitat quality distribution of juvenile Chinook salmon within the Lemhi River (Eastern Idaho, USA). Modeling results showed two key aspects: (1) a reduction in diverted flows is not sufficient to improve habitat quality potentially because of a legacy of morphological simplification (directly due to straightening and wood removal and indirectly due to low in-channel flows) and (2) morphological complexity and connectivity with side channels and margin areas are key and vital elements to support suitable habitats that meet or exceed energetic needs to sustain or promote growth of individuals and populations.

Introduction

As global human population rise continues, pressure on freshwater resources increases (Davis et al. 2015). An ever-changing climate scenario, coupled with human population growth and its impacts, has begun to put strain on already vulnerable freshwater ecosystems (Woodward et al. 2010). Worldwide concern for conservation of biological diversity and the necessity to limit species loss across the planet has been recognized in both the scientific community (Rand et al. 2012; Isaak et al. 2017) and legislation worldwide (Hering et al. 2010). Native, anadromous fishes, which access freshwater for portions of their life history (Healey 1992) face analogous pressures to global freshwater ecosystems and are in consistent decline, with some populations facing immediate extinction threats (Gustafson et al. 2007). Likewise, local populations, such as those found in the Pacific Northwest of the United States, may rest on tributary restoration, and land use changes for recovery (NOAA 2008; NOAA 2011; NMFS 2014). However, our ability to appropriately restore and monitor restoration success and land recovery is uncertain (Bernhardt 2005; Schwartz 2016).

Enhancement of stream habitat has begun to focus on more process-based approaches for restoration to promote and sustain function (Moir et al. 2010; Wohl et al. 2015). Restorative, natural processes,

may require floodplain reconnection, side channel construction or enhancement, and development of complex habitat provided by wood or other structures in order to provide benefit for multiple life stages and target species (Bisson et al. 2009; Bennett et al. 2016; Roni et al. 2018; Bond et al. 2018). Therefore, improvement of modeling and monitoring techniques is necessary to better characterize ecological uplift in select areas identified for effective habitat enhancement. The shortcomings of current fish-habitat modeling techniques are widely evaluated and documented, where links between water use, nutrient availability, and habitat suitability are continuously being explored and further understood, but our ability to understand these links has remained intangible (Schwartz 2016).

Various methods to quantify aquatic habitat quality and quantity have been employed in freshwater ecology and fisheries: from individual based models (IBM) (Goodwin et al. 2006) assessing impacts and interactions of juvenile fish at dams, micro habitat assessments of salmon nesting patterns (McKean et al. 2008; Benjankar et al. 2016; Kammel et al. 2016), to macro-scale basin wide analysis (Isaak and Thurow 2006) and monitoring of habitat patterns and trends (Cohen et al. 1998; Newson and Newson 2000; Bond et al. 2018). Model inputs have varied with model choice, where multiple univariate inputs such as depth and velocity combined with habitat preference and suitability curves have been used (Benjankar et al. 2015) or furthered by multivariate fuzzy inference approaches attempting to account for interactions of instream habitat characteristics such as depth, velocity, and substrate distribution (Jorde et al. 2001; Noack et al. 2013). With recent advances and understanding of fish energetic balance and incorporation of data such as temperature (Benjankar et al. 2018) and food availability (Keeley et al. 2016), one emergent technique for development of fish-habitat relationships has taken shape as bioenergetic modeling.

Many bioenergetic models aim to assess the amount of suitable habitat for stream dwelling fishes through suitability calculations, growth rates, or nutrient availability as indicators of the viability of target species to maintain permanence within a given watershed or system (Chittaro et al. 2014; Keeley et al. 2016; Wall et al. 2016). Thus far, limitations in necessary continuous data have restricted usage of bioenergetics modeling to simple channel unit and cross-sectional analysis (Hayes et al. 2007; Wall et al. 2016). Recent advances in both remote sensing and numerical flow modeling may help to eliminate some constraints. In remote sensing, the advent of topobathymetric LiDARs allows mapping the riverscape at the meter scale, over hundreds of kilometers of stream length, with centimeter accuracy, removing the spatial limitations on continuous coverage of stream geometry (Tonina et al. 2018). Coupling high resolution bathymetry with two-dimensional numerical modeling of flow hydraulics allows for the derivation of continuous information of flow hydraulics and water quantities (McKean and Tonina 2013).

Here we applied these advances to support an energetic mass balance modeling approach (Jenkins and Keeley 2010; Keeley et al. 2016) to assess and understand the impact of water use, water quality, and anthropogenic stream morphological (straightening and restoration) changes on aquatic habitat quality distribution. Our goal is to present a new framework built on process-based models to investigate aquatic ecosystems broadly across watersheds. We applied this framework to three distinct ~1 km long (60 bankfull channel widths) reaches of the upper Lemhi River (Eastern Idaho, USA). The Lemhi watershed is an ideal study area to test such an approach because it supports endangered populations of anadromous fishes, under strong anthropogenic influences of water use and habitat alteration, and has readily available spatially continuous data including: LiDAR supported bathymetry, discharge measurements, drift macroinvertebrate sampling, temperature measurements, and juvenile fish capture.

Methods and Materials

Study Site

The Lemhi River is a tributary of the Salmon River approximately 100 km long between its origin near the town of Leadore, (Idaho, USA) and its confluence with the Salmon River, near the town of Salmon (Idaho, USA). Its drainage area encompasses 3,300 km^2 of forest, range, and irrigated farm land. The basin supports wild populations of threatened Chinook salmon (*Oncorhynchus tshawytscha*) and steelhead trout (*O. mykiss*), listed under the U.S. Endangered Species Act (NMFS, 2014). Chinook salmon of the Columbia River basin (where the waters of the Lemhi eventually flow), provide significant socioeconomical benefit including; food production for commercial fishing, recreational fishing, subsistence fishing, and nutrient cycling services, and are of important social and cultural value (Morton et al. 2017). The Lemhi River boasts a full range of Chinook salmon life stages beginning with a return of spawning adults in the spring (spawning in the late summer/early fall), juvenile emergence in March, over-winter rearing of juvenile Chinook parr and pre-smolts, to an outmigration of age-1 smolts in the spring (Bjornn 1971). Yet, large amounts of water withdrawal for irrigation during the agricultural growing season, between May and October, have drastic impacts on stream habitat and the ecosystem of the Lemhi basin; shifting flow timing, lowering critical summer flow, and potentially reducing habitat quality for key life stages (Walters et al. 2013). Anthropogenic activities have also changed the stream alignment, via straightening and floodplain connectivity by removing and limiting lateral channels.

Study Reaches

We chose three reaches in the upper Lemhi River, each approximately 1 km long to model the bioenergetic profitability for juvenile Chinook salmon (Figure 2.-1; Figure 2-2). The three study

reaches were selected to represent a broad range of morphologies typically encountered in a meadow system: with a mix of straight, meandering, and multi-thread systems including an engineered restored reach. These reaches are also in close proximity to one another such that they had similar discharge, stream water temperature and macroinvertebrate drift rates.

The upstream most reach, referenced as the Straight reach, is a single thread, straight, nearly trapezoidal, simplified channel, confined in parts by a highway that parallels this section. The middle reach, referred to as the Complex reach, is a multi-threaded channel with side branches and meanders within a meadow setting. The reach has variable amounts of streamside vegetation and instream habitat conditions. The downstream most reach is an engineered, restored channel referred to as the Engineered reach. The channel was completely re-designed and engineered as a restoration project. The engineered channel is a new reach dug in the floodplain and the pre-restoration straight channel was abandoned and closed off. For this restored section, we modeled two scenarios: 1) as a two-thread system with the pre-restoration, straight channel functioning as a side channel, called the Restoration Open reach where the two channels are open and functioning in parallel and 2) as a single thread system without a side channel, called the Restoration Closed reach. In the former case, flow splits between the two reaches depending on the local geometry of the system. The natural diversion of the flow between the two channels allowed us to quantitatively compare results between these two restoration scenarios.

Each study reach experiences large amounts of upstream dewatering via diversions for agricultural production. We chose to model two flow (diverted and undiverted) regimes and two temporal periods for each reach of interest, resulting in a total of 4 scenarios through 4 distinct reaches.

Modeled Scenarios

To assess the effects of water use for all reaches, we modeled both a diverted and an undiverted flow condition for two critical periods: late summer (August), and fall (October) (Figure 2-3). A late August period was selected because all water diversions are typically in use, discharge is near the lowest volume of the year, and water stream temperatures are high (weekly average ~12° C). Conversely, the last part of October has all diversions closed, hydrology follows a natural flow regime, and stream water temperatures are still warm and relatively mild (weekly average ~7° C) with fish feeding and rearing. Late October has been suggested to be a critical period as many young rearing fish leave the Lemhi as pre-smolts, to the Salmon River (Copeland et al. 2014), indicating that habitat may not be suitable for pre-smolt fish.

To test the impacts of water management and flow hydraulics on our study reaches (e.g., depth and velocity) we held all input parameters constant except for discharge for two alternative flow scenarios: 1) for a more natural flow regime during August, we chose the same discharge volume as October and 2) to test an alternative water management scenario for October, we modeled a reduced discharge equal to that of August. These alternative scenarios allowed us to estimate the change in suitable area as a function of water management alone.

Modeling

The modeling can be explained as a two-step approach. First, we developed and validated a 2-dimensional numerical flow model supported by high resolution bathymetry to model depth and velocity at a 1 m resolution across each study reach. Second, we then used depth and velocity and combined them with available biological information including temperature, aquatic invertebrate drift rate, and juvenile Chinook salmon size distributions to populate a spatially explicit bioenergetics model across all our modeling scenarios and reaches.

Hydraulic Modeling

High Resolution Topobathymetric Surface

Bathymetric LiDAR data were collected in the Fall of 2013 (Tonina et al. 2018) with the Experimental Advanced Airborne Research LiDAR-B (EAARL-B) sensor for the entire mainstem Lemhi River. From the original point cloud, a 1 m digital elevation model, DEM, was derived for both stream and floodplain topographies. The DEM was extensively validated by comparing LiDAR survey with a high resolution, high accuracy differential global positioning system (D-GPS) real time kinematic (RTK) survey instruments at 3 test-beds with high resolution (1.6 points/m^2) which showed root mean square error, RMSE, and median absolute error (M), of 0.11 m for the submerged topography (Tonina et al. 2018) and at 454 centerline points spaced evenly along the upper 25 km of the dataset with RMSE and M slightly higher at 0.13 m.

Numerical Flow Model

A calibrated and validated 2-dimensional hydraulic model (Danish Hydraulics Institute Mike 21; DHI, 2000) supported by a 1 m resolution DEM derived from the bathymetric LiDAR survey, serving as the defined boundary condition, quantified stream water depths and depth-averaged velocities for the modeled discharges. The numerical model solves the 2-dimensional Reynolds averaged Navier-Stokes Equations with the Boussinesq turbulence closure (DHI, 2000). It has 2 coefficients that need to be assigned: lateral eddy viscosity constant and Manning's *n*. Both coefficients were set as spatially constant, the former with a constant value of 0.15 m^2/s, the latter of 0.025 $s/m^{1/3}$ for the entire system. The Manning's *n* value was selected by minimizing the RMSE between measured and

predicted depth-averaged velocity and water surface elevation. The RMSE for velocity was 0.19 m/s and for water surface elevation was 0.03 m at low summer discharges (around 2 m^3/s) at the test-bed locations where the DEM was analyzed. The selected Manning's *n* was then validated by comparing measured water surface elevation (with Real Time Kinematic Digital Global Positioning System) and depth-averaged flow velocity (with an Acoustic Doppler Velocimeter) collected at different discharges during late October (still low to guarantee safety during measurements but higher, approximately double, from those of the calibration) and locations along the upper 32 km of the Lemhi River where the 3 study sites were located. Validation of the model resulted in RMSEs of 0.11 m, 0.18 m and 0.2 m/s, for water surface elevation, depth and velocity, respectively. These calibration and validation results were within published acceptable values for numerical flow modeling (Kammel et al. 2016).

Flow Scenarios

The 2-dimensional model was run for a set of representative discharges, which spanned the daily mean hydrograph recorded for the Lemhi River at Cottom Lane, Idaho Department of Water Resources (IDWR) gauging station, located just downstream of the study reaches. From this set of discharges, we selected those closer to the mean weekly average discharges of the last weeks of August (2 m^3/s) and October (5 m^3/s) (Figure 2-3).

Bioenergetics/Foraging Model

Feeding Stations

Feeding locations for juvenile Chinook salmon were generated using a geographic information system (GIS) software (ESRI ArcGIS 10.6). We constructed cross sections perpendicular to the centerline of all wetted channels (including main and off-channel areas consisting of side channels and backwaters) for each reach at 3 m intervals to reduce overlap in sharp meander bends. We then generated points every 1 m along each individual cross section. We chose to generate points every 1 m to match the 1 m by 1 m resolution of the modeled depth and velocity output rasters. We then performed an Extract Value to Point (ESRI, 2017) with the constructed feeding locations and modeled output rasters to extract depth and velocity values at each individual feeding point location.

Bioenergetics Model

To calculate the bioenergetic profitability of each feeding station/point location within our study reaches we used a foraging model originally developed by Hughes and Dill (1990) to calculate net energy intake (NEI) which was then further developed and tested by Guensch et al. (2001) and Jenkins and Keeley (2010) and then again applied by Keeley et al. (2016). The model input variables consist of water depth and depth-averaged velocity, juvenile Chinook salmon fork length and mass,

drift rate binned by size class, stream water temperature, and feeding locations. The model assesses the amount of energy freely available in the stream, minus the cost of capture, swimming, metabolism, and excretion following the relationships described in Jenkins and Keeley (2010) and Keeley et al. (2016).

To convert the calculated NEI_i value to an assessment of suitability, we calculated a required maintenance energetic requirement (ration), MR_i for the *i*-th percentile of fork length and mass of captured juvenile Chinook modeled. The ratio, defined available energy for growth, AE_i, between the local NEI_i value and the maintenance ration to provide an index of habitat suitability:

$$AE_i = \frac{NEI_i}{MR_i}$$

such that values of AE_i less than 1 indicate that feeding location is unsuitable for growth as it consumes more energy than its critical value, conversely, values larger than one indicate that the feeding location promotes growth. A value of 1 indicates that the location maintains the same size of the fish.

Temperature

Stream water temperatures along the Lemhi River were collected with in-stream deployed Onset Hobo Tidbits by the Columbia Habitat Monitoring Program (CHaMP, 2014). The nearest monitoring site was approximately 1 km downstream of the study sites. We quantified the weekly average temperature of the last week of August 2016, and October 2016 from hourly temperature observations as input information for the bioenergetic model.

Juvenile Chinook Salmon Length and Mass

We obtained all length and mass information of juvenile Chinook salmon from the publicly available dataset developed as part of the Integrated Status Effectiveness Monitoring Program (ISEMP). The dataset contains information collected from both electrofishing mark recapture studies and rotary screw operations in the Lemhi River watershed. We calculated the 25th, 50th, 75th, and 90th percentile of fork length for juvenile Chinook salmon from the available fish data to identify the range of fish sizes that were modeled in the bioenergetic evaluation of habitat quality for each study reach. We used a linear regression model (M_{fish}=3.18 F_l -5.24, R^2=0.96) to quantify the relationship between fork length and fish mass to calculate the mass of each *i*-th percentile of observed fork lengths where F_l is equal to the measured fork length of interest and M_{fish} is the mass of the given fish at a given fork length.

Drift Density

To estimate food availability for juvenile salmon, we used samples of invertebrates drifting in the water column collected during daylight hours. Counts of captured, drifting macroinvertebrates were obtained from the habitat evaluation program CHAMP (CHaMP, 2014; Bouwes et al. 2011). Precautions during net deployment were taken to ensure that benthic invertebrates did not crawl into the net, and deployment timing occurred during optimal conditions, avoiding crepuscular periods (Weber et al. 2014; Wheaton et al. 2018). The captured drifting invertebrates were binned into 4 equal length size class bins (mm) and the total volume of water calculated/sampled was used to create a drifting rate of invertebrates, where the total number of invertebrates captured in each size class was divided by the total volume of water sampled. We used the available CHaMP data from the site most closely located to our three reaches to generate drift rates needed to model food availability for the bioenergetic calculations of habitat quality.

Analysis

The first step in analyzing the bioenergetic results was to calculate the fraction of feeding stations that either met or exceeded the maintenance ration, $AE \geq 1$ (Figure 2-5). We did so for each reach/scenario, and all modeled fork lengths. Because the difference in percent suitable for each fork length was marginal and due to the computational time to run each model, we only preceded in further analysis with modeling the 50th percentile of fish size, which corresponded to a fish size of 75 mm as an estimate of the average size of juvenile Chinook salmon in the Lemhi River.

We analyzed *AE* both as statistical values via frequency distribution, which allowed comparison among sites, and as spatial information as maps. The latter allowed us to analyze the spatial distribution of *AE* and visualize correlation between hydro-morphological variables and *AE* values. We separated the analysis into the main channel and side channels to gain an understanding of the contributing total area of suitable habitat by the off-channel areas. We calculated the wetted areas of main and off-channel areas and then multiplied these values by the fraction of feeding locations that met or exceeded the maintenance ration, $AE \geq 1$. This result provided us with an estimate of suitable area for the main and off-channel habitat. To assess the percent of area that the off-channel contributed to the total suitable area, we divided the total off-channel suitable area by the reach total suitable area for each modeled scenario to estimate the percent contributing suitable area by the off-channel.

Results

During the August scenario, all reaches exhibited greater than 95% of their area where $AE \geq 1$ with several scenarios approaching 100% of the total area suitable regardless of main and off-channel

location or presence. Suitability expressed as percent of area that met or exceeded a maintenance ration of energy intake, with $AE \geq 1$ slightly increased with fork length for the August fully diverted scenario in all reaches (Figure 2-4). Conversely, during the undiverted, late October scenario, the proportion of suitable habitat decreased sharply for all fork lengths compared to the results from the August modeled scenario. The fraction of suitable habitat also decreases in all reaches for the undiverted October time period with increasing fork length of fish (Figure 2-4). The sharp decrease in areas with $AE \geq 1$ from August to October is most notable in the main channel of each reach (Figure 2-5). During late October, the only remaining suitable habitat is near the margins of the main channel, and off-channel areas consisting of side channel and backwater habitat. The Complex and Restoration Open reaches have the greatest amount of high-quality habitat for both scenarios modeled, August and October (Figure 2-6). The largest fraction of $AE > 1$ is found in the Complex reach and the Restoration Open scenario, in addition to the largest fraction of area where $AE > 3$.

The impacts of off-channel habitat for each modeled reach, for 75 mm Chinook salmon (50^{th} percentile fish size for the Lemhi River) suggests that the Complex and Restoration Open reaches have the highest percentage and amount (m^2) of suitable off-channel habitat for both the August and October flow scenarios (Figure 2-7; Figure 2-8). Within the three modeled reaches that contain off-channel habitat, all exhibit a decline in the percent of suitable habitat from the August to October flow scenario (Figure 2-7). With regards to the total suitable area (m^2), all reaches have a sharp decline from August to the October flow regime. The Complex and Restoration Open reaches have the greatest amount of off-channel suitable habitat, followed by the Restoration Closed reach. The straight reach contains no off-channel habitat and thus the off-channel does not contribute to the total area of suitable habitat. The Restoration Open reach has the second most area of suitable habitat in total and in the off-channel, followed by the Restoration Closed scenario, and lastly the Straight reach.

The contributing percentage of off-channel habitat to the total area of suitable habitat increases from the August to the October flow scenarios in each modeled reach with side channels (Figure 2-8). Both, the Complex and Restoration Open reaches have the largest proportion of suitable off-channel habitat contributing to the total suitable habitat, with the Restoration Open reach having the greatest amount for both modeled flow scenarios. The Straight reach does not contain any off-channel habitat, therefore the resulting percent contributing to the total is zero. The undiverted, late summer, alternative flow scenario (increased discharge), decreased the percent of the total suitable area in all reaches (Figure 2-9), with the straight reach having the greatest percent in reduction, followed by the Restoration Closed reach and the Restoration Open illustrating the least amount of percent reduction.

Similarly, the late October undiverted flows had lower suitable area than that of the decreased, diverted discharge scenario (Figure 2-10).

Discussion

To improve channel function and habitat complexity, floodplain reconnection and side channel construction may be necessary to restore natural, sustainable processes (Bisson et al. 2009; Roni et al. 2018). The Columbia River basin has experienced a loss of floodplain habitat and our results help support the assumption that in general, watersheds throughout the western United States would benefit from floodplain enhancements (Bond et al. 2018). Further, restoring channel function through side channel construction will help mitigate habitat loss for juvenile Chinook salmon (Figure 2-5; Figure 2-8). Our study and similar types of analyses may also help provide insight into the cost-benefit of channel enhancement through pre and post restoration modeling as a function of the change in suitable area (Figure 2-7).

The undiverted summer scenarios predict that as water is returned to the channel through tributary reconnections, minimum flow requirements, and reduction in diversion volumes due to changes in irrigation practices, an already simplified channel may not have the morphology to provide suitable habitat for juvenile salmonids. Simplified morphology includes subdued geometry, such as shallow pools or low-amplitude riffles, but also lack or contain limited connectivity with lateral channels (off-channel) and marginal habitats. Reaches with complex features such as margin habitat and side channels maintain suitable habitat at high flow and in our case, buffer the decline in overall suitability reduction from August to October. As diverted water volumes are decreased, a simultaneous effort should focus on restoring channel processes, including reconnection and engineering of secondary and back water channels (Wohl et al. 2015).

A previous study of fish bioenergetics showed that cutthroat trout preferred slower, deeper, pool habitat, where greater NEI values were calculated (Jenkins and Keeley 2010). Our results support this finding, where areas of slower water and lower flow periods have a higher calculated NEI and a greater amount of suitable habitat for juvenile Chinook salmon. These suitable habitats are observed when the engineered and the original main channel are allowed to function as a two-thread system rather than diverting flow solely into the engineered channel (Figure 2-4; Figure 2-5). Further, our alternate water management scenario demonstrates that when return flows are moderated, this results in a greater estimated area of suitable habitat (Figure 2-10). Increasing channel flow should be accompanied by a restoration of channel form (Palmer et al. 2010) and restoration projects must consider multiple flow scenarios and life stages of target species to better address limiting factors within watersheds (Schwartz 2016) (Figure 2-9).

Several studies within the Lemhi River basin have shown that streamflow can be used as a good predictor of juvenile survival to the ocean (Arthaud et al. 2010; Walters et al. 2013). During a climate change scenario, modeled to 2040, Arthaud et al. (2010) estimated that undiverted streamflow projected to increase juvenile survival by 42-58%. In addition, tributary flow during early rearing was found as a good predictor of survival/productivity, but mainstem Columbia River flow was estimated as the best predictor (Walters et al. 2013). Conversely, our study shows that high flows may decrease the amount of available habitat suitable for juvenile fish. From August low (fully diverted water) to October (fully undiverted water) the overall bioenergetic suitability of our study reaches declined drastically, mainly due to increase in velocities rather than change in water temperatures (Figure 2-4; Figure 2-5; Figure 2-6). Walters et al. (2013) only assessed change in habitat capacity as a result of the change in channel area due to increased flow from removal of diversions, whereas our model incorporates not only spatially distributed depths and velocities, but also temperature and food availability in quantifying the habitat quality for juvenile Chinook salmon. Our result parallels what Jenkins and Keeley (2010) reported; fish in the Salmon River basin can maintain high growth rates during the summer months, but habitat suitability might decline in October. The reduction in suitable habitat may be the cause explaining the outmigration of many juvenile Chinook salmon in the Lemhi basin in the Fall as pre-smolts (Bjornn 1971; Copeland et al. 2014) rather than the following spring as true 1-year old smolts. This may also help characterizing why juvenile to adult return rates are better predicted by mainstem down river flow rather than tributary flow (Arthaud et al. 2010).

Limitations in this type of modeling have been documented and improvements to modelling have been suggested (Hayes et al. 2007; Jenkins and Keeley 2010; Wall et al. 2016). Wall et al. (2016) overpredicted salmonid carrying capacity of their study sites when model estimates were validated against measured fish densities. In our study, the overestimations of habitat quality could be a function of the calculated maintenance ration, where this equation was originally developed for brown trout and may not characterize the energetic needs of Chinook salmon properly. Although, other studies have used this technique (e.g., Jenkins and Keeley 2010; Keeley et al. 2016) more research may be needed to derive a juvenile Chinook salmon maintenance ration. Parallel to Wall et al. (2016), we assumed that drift was spatially evenly distributed throughout all reaches and it is likely that this is not the case. We did not account for drift depletion due to foraging from other species or competition among the same modeled species. Yet, our measured drift rates were well within limits reported by other studies of 1 to 5 invertebrates per cubic meter to as many as 20 to 50 invertebrates per cubic meter (Allan 1978; Wilzbach and Hall 1985; Leung et al. 2009; Jenkins and Keeley 2010). Additional limitations may include inherent error in the numerical modeling process and outputs, however studies have shown that 2-dimensional numerical modeling, and LiDAR

supported numerical modeling are sufficient to generate distributed depths and velocities (McKean et al. 2014; Tonina et al. 2018).

One improvement to the depth and velocity models might rely on better accuracy and higher resolution LiDAR supported topobathymetry, allowing us to model at finer than 1 m resolution (Tonina et al. 2018). Model development and analysis such as this was driven by freely available data, where the data driving this study (fish size, drift rates, temperature, LiDAR data) was all feely available and accessible. It is extremely important that open source data continue to be developed to push the understanding of biotic and mechanistic linkages that govern fish behavior and recovery. This type of modeling approach may also be improved and more widely applicable to other science driven questions and management scenarios so long as information is continued to be made public.

Conclusion

Understanding the complex feedback among habitat degradation, water and land use, restoration activities and strategies, and the outcome predictions of such activities on ecosystem status in freshwater river systems requires holistic and fine-resolution modeling techniques, which have not been available. To address this knowledge gap, we developed a novel approach to bioenergetics modeling, which leveraged new topobathymetric LiDAR technology, multidimensional numerical flow modeling, and fisheries and habitat data. This new approach allowed for the assessment of morphological impacts and water use on juvenile Chinook salmon habitat suitability. Our modeling demonstrates that removing diversions, and thus returning the flow regime to its natural condition is not sufficient to revert the impact of anthropogenic activities and may be detrimental in the short period without simultaneously focusing on in-channel morphology. Water diversion reduction towards natural flows needs to be accompanied by increasing lateral connectivity and main channel flow complexity. Anthropogenically simplified, main stem areas currently have flow velocity too fast to maintain bioenergetic conditions that support growth for a natural flow regime.

Our results highlight the importance of restoration activities that reconnect the main channel to/and construct lateral habitat, develop slow water areas, and increase the overall channel length to increase the total suitable area as flow approaches natural conditions. Increase in flow complexity and preserving local low velocities could be achieved with both abiotic and biotic strategies and their combination. The former could include reintroduction of large woody debris, reconnection of side channels, followed by adequate maintenance flows, and the latter with healthy riparian vegetation, which produce natural wood recruitment and reintroduction of native riverine mammals like beavers. These strategies may provide process driven channel scour and lateral movement into the flood plain that could help increase overall suitable area. Though, not all strategies are adequate for all streams,

an approach as that proposed in this study could help identify the most suitable life-stage specific set of solutions.

This study further demonstrates the utility of remotely sensed topobathymetry and LiDAR-supported numerical flow modeling, meanwhile building upon biological-data supported bioenergetic modeling to assess water use and channel simplification on aquatic habitat distribution beyond the traditional limited reach scale (10-20 bankfull channel widths or a few hundred meters). These results and methodologies could be adapted and applied to other watersheds to gain more comprehensive understanding and address limiting factors to help ecosystem recovery or guide development of new ecosystems. Studies such as this, allow for development of a virtual stream where processes can be studied at the proper resolution and length scale and alternative strategies can be evaluated. Whereas, returning the natural flow regime (removing diversion in this case) without adequate morphological enhancements may not lead to the expected restoration outcomes in the short term but could even be detrimental, it may have beneficial effects at the long time scale. At an extended time scale, decades, stream morphology will readjust to the hydrological and sediment input regime. This suggests that restoration activities should evaluate both short and long term effects of re-establishing a near natural flow and whether passive (without morphological restoration), enhancement (small morphological changes in at hoc location) and active (with morphological adjustment) restorations would be better for the goals and expected outcomes.

Literature Cited

Allan, J.D. 1978. Trout predation and the size composition of stream drift 1. Limnol. Oceanogr. **23**(6): 1231–1237. doi:10.4319/lo.1978.23.6.1231.

Arthaud, D.L., Greene, C.M., Guilbault, K., and Morrow, J. V. 2010. Contrasting life-cycle impacts of stream flow on two Chinook salmon populations. Hydrobiologia **655**(1): 171–188. doi:10.1007/s10750-010-0419-0.

Benjankar, R., Tonina, D., Marzadri, A., McKean, J., and Isaak, D.J. 2016. Effects of habitat quality and ambient hyporheic flows on salmon spawning site selection. J. Geophys. Res. G Biogeosciences **121**(5): 1222–1235. doi:10.1002/2015JG003079.

Benjankar, R., Tonina, D., and Mckean, J. 2015. One-dimensional and two-dimensional hydrodynamic modeling derived flow properties: Impacts on aquatic habitat quality predictions. Earth Surf. Process. Landforms **40**(3): 340–356. doi:10.1002/esp.3637.

Benjankar, R., Tonina, D., McKean, J.A., Sohrabi, M.M., Chen, Q., and Vidergar, D. 2018. Dam

operations may improve aquatic habitat and offset negative effects of climate change. J. Environ. Manage. **213**: 126–134. doi:10.1016/j.jenvman.2018.02.066.

Bennett, S., Pess, G., Bouwes, N., Roni, P., Bilby, R.E., Gallagher, S., Ruzycki, J., Buehrens, T., Krueger, K., Ehinger, W., Anderson, J., Jordan, C., Bowersox, B., and Greene, C. 2016. Progress and Challenges of Testing the Effectiveness of Stream Restoration in the Pacific Northwest Using Intensively Monitored Watersheds. Fisheries **41**(2): 92–103. doi:10.1080/03632415.2015.1127805.

Bernhardt, E.S. 2005. ECOLOGY: Synthesizing U.S. River Restoration Efforts. Science (80-.). **308**(5722): 636–637. doi:10.1126/science.1109769.

Bisson, P.A., Dunham, J.B., and Reeves, G.H. 2009. Synthesis, part of a Special Feature on Pathways to Resilient Salmon Ecosystems Freshwater Ecosystems and Resilience of Pacific Salmon: Habitat Management Based on Natural Variability. Ecol. Soc. **14**(1). doi:10.5751/ES-02784-140145.

Bjornn, T.C. 1971. Trout and Salmon Movements in Two Idaho Streams as Related to Temperature, Food, Stream Flow, Cover, and Population Density. Trans. Am. Fish. Soc. **100**(3): 423–438. doi:10.1577/1548-8659(1971)100<423:TASMIT>2.0.CO;2.

Bond, M.H., Nodine, T.G., Beechie, T.J., and Zabel, R.W. 2018. Estimating the benefits of widespread floodplain reconnection for Columbia River Chinook salmon. Can. J. Fish. Aquat. Sci.: 1–15. doi:10.1139/cjfas-2018-0108.

Chittaro, P.M., Zabel, R.W., Haught, K., Sanderson, B.L., and Kennedy, B.P. 2014. Spatial and temporal patterns of growth and consumption by juvenile spring/summer Chinook salmon Oncorhynchus tshawytscha. Environ. Biol. Fishes **97**(12): 1397–1409. doi:10.1007/s10641-014-0230-2.

Cohen, P., Andriamahefa, H., and Wasson, J.-G. 1998. Towards a regionalizaton of aquatic habitat: distribution of mesohabitats at the scale of a large basin. Regul. Rivers Res. Manag. **14**(1): 391–404. doi:10.1002/(SICI)1099-1646(199809/10)14:5<391::AID-RRR513>3.0.CO;2-W.

Copeland, T., Venditti, D.A., and Barnett, B.R. 2014. The Importance of Juvenile Migration Tactics to Adult Recruitment in Stream-Type Chinook Salmon Populations. Trans. Am. Fish. Soc. **143**(6): 1460–1475. doi:10.1080/00028487.2014.949011.

Davis, J., O'Grady, A.P., Dale, A., Arthington, A.H., Gell, P.A., Driver, P.D., Bond, N., Casanova,

M., Finlayson, M., Watts, R.J., Capon, S.J., Nagelkerken, I., Tingley, R., Fry, B., Page, T.J., and Specht, A. 2015. When trends intersect: The challenge of protecting freshwater ecosystems under multiple land use and hydrological intensification scenarios. Sci. Total Environ. **534**: 65–78. Elsevier B.V. doi:10.1016/j.scitotenv.2015.03.127.

Goodwin, R.A., Nestler, J.M., Anderson, J.J., Weber, L.J., and Loucks, D.P. 2006. Forecasting 3-D fish movement behavior using a Eulerian-Lagrangian-agent method (ELAM). Ecol. Modell. **192**(1–2): 197–223. doi:10.1016/j.ecolmodel.2005.08.004.

Guensch, G.R., Hardy, T.B., and Addley, R.C. 2001. Examining feeding strategies and position choice of drift-feeding salmonids using an individual-based, mechanistic foraging model. Can. J. Fish. Aquat. Sci. **58**(3): 446–457. doi:10.1139/f00-257.

Gustafson, R.G., Waples, R.S., Myers, J.M., Weitkamp, L.A., Bryant, G.J., Johnson, O.W., and Hard, J.J. 2007. Pacific salmon extinctions: Quantifying lost and remaining diversity. Conserv. Biol. **21**(4): 1009–1020. doi:10.1111/j.1523-1739.2007.00693.x.

Hayes, J.W., Hughes, N.F., and Kelly, L.H. 2007. Process-based modelling of invertebrate drift transport, net energy intake and reach carrying capacity for drift-feeding salmonids. Ecol. Modell. **207**(2–4): 171–188. doi:10.1016/j.ecolmodel.2007.04.032.

Healey, M.C. 1992. Life history of Chinook Salmon (Oncorhynchus tshawytscha). *In* Pacific Salmon Life Histories. doi:10.2307/1446178.

Hering, D., Borja, A., Carstensen, J., Carvalho, L., Elliott, M., Feld, C.K., Heiskanen, A.-S., Johnson, R.K., Moe, J., and Pont, D. 2010. The European Water Framework Directive at the age of 10: A critical review of the achievements with recommendations for the future. Sci. Total Environ. **408**(19): 4007–4019. doi:10.1016/j.scitotenv.2010.05.031.

Hughes, N.F., and Dill, L.M. 1990. Position Choice by Drift-Feeding Salmonids: Model and Test for Arctic Grayling (Thymallus arcticus) in Subarctic Mountain Streams, Interior Alaska. Can. J. Fish. Aquat. Sci. **47**(10): 2039–2048. doi:10.1139/f90-228.

Isaak, D.J., and Thurow, R.F. 2006. Network-scale spatial and temporal variation in Chinook salmon (Oncorhynchus tshawytscha) redd distributions: patterns inferred from spatially continuous replicate surveys. Can. J. Fish. Aquat. Sci. **63**(2): 285–296. doi:10.1139/f05-214.

Isaak, D.J., Wenger, S.J., Peterson, E.E., Ver Hoef, J.M., Nagel, D.E., Luce, C.H., Hostetler, S.W., Dunham, J.B., Roper, B.B., Wollrab, S.P., Chandler, G.L., Horan, D.L., and Parkes-Payne, S.

2017. The NorWeST Summer Stream Temperature Model and Scenarios for the Western U.S.: A Crowd-Sourced Database and New Geospatial Tools Foster a User Community and Predict Broad Climate Warming of Rivers and Streams. Water Resour. Res. **53**(11): 9181–9205. doi:10.1002/2017WR020969.

Jenkins, A.R., and Keeley, E.R. 2010. Bioenergetic assessment of habitat quality for stream-dwelling cutthroat trout (Oncorhynchus clarkii bouvieri) with implications for climate change and nutrient supplementation. Can. J. Fish. Aquat. Sci. **67**(2): 371–385. doi:10.1139/F09-193.

Jorde, K., Schneider, M., Peter, A., and Zoellner, F. 2001. Fuzzy based Models for the Evaluation of Fish Habitat Quality and Instream Flow Assessment. Proc. 3rd Int. Symp. Environ. Hydraul. 5–8 December, Tempe, AZ (January): 1–6.

Kammel, L.E., Pasternack, G.B., Massa, D.A., and Bratovich, P.M. 2016. Near-census ecohydraulics bioverification of *Oncorhynchus mykiss* spawning microhabitat preferences. J. Ecohydraulics **1**(1–2): 62–78. Taylor & Francis. doi:10.1080/24705357.2016.1237264.

Keeley, E.R., Campbell, S.O., and Kohler, A.E. 2016. Bioenergetic calculations evaluate changes to habitat quality for salmonid fishes in streams treated with salmon carcass analog. Can. J. Fish. Aquat. Sci. **73**(5): 819–831. doi:10.1139/cjfas-2015-0265.

Leung, E.S., Rosenfeld, J.S., and Bernhardt, J.R. 2009. Habitat effects on invertebrate drift in a small trout stream: implications for prey availability to drift-feeding fish. Hydrobiologia **623**(1): 113–125. doi:10.1007/s10750-008-9652-1.

McKean, J., and Tonina, D. 2013. Bed stability in unconfined gravel bed mountain streams: With implications for salmon spawning viability in future climates. J. Geophys. Res. Earth Surf. **118**(3): 1227–1240. doi:10.1002/jgrf.20092.

McKean, J., Tonina, D., Bohn, C., and Wright, C.W. 2014. Effects of bathymetric lidar errors on flow properties predicted with a multi-dimensional hydraulic model. J. Geophys. Res. Earth Surf. **119**(3): 644–664. doi:10.1002/2013JF002897.

McKean, J.A., Isaak, D.J., and Wright, C.W. 2008. Geomorphic controls on salmon nesting patterns described by a new, narrow-beam terrestrial-aquatic lidar. Front. Ecol. Environ. **6**(3): 125–130. doi:10.1890/070109.

Moir, H., Beechie, T.J., Sear, D.A., Roni, P., Pollock, M.M., Pess, G.R., Olden, J.D., and Buffington, J.M. 2010. Process-based Principles for Restoring River Ecosystems. Bioscience **60**(3): 209–

222. doi:10.1525/bio.2010.60.3.7.

Morton, C., Knowler, D., Brugere, C., Lymer, D., and Bartley, D. 2017. Valuation of fish production services in river basins: A case study of the Columbia River. Ecosyst. Serv. **24**: 101–113. Elsevier B.V. doi:10.1016/j.ecoser.2017.02.007.

Newson, M.D., and Newson, C.L. 2000. Geomorphology, ecology and river channel habitat: Mesoscale approaches to basin-scle chailenges. Prog. Phys. Geogr. **24**(2): 195–217. doi:10.1177/030913330002400203.

Noack, M., Schneider, M., and Wieprecht, S. 2013. The Habitat Modelling System CASiMiR: A Multivariate Fuzzy Approach and its Applications. Ecohydraulics An Integr. Approach: 75–91. doi:10.1002/9781118526576.ch4.

Palmer, M.A., Menninger, H.L., and Bernhardt, E. 2010. River restoration, habitat heterogeneity and biodiversity: A failure of theory or practice? Freshw. Biol. **55**(SUPPL. 1): 205–222. doi:10.1111/j.1365-2427.2009.02372.x.

Rand, P.S., Goslin, M., Gross, M.R., Irvine, J.R., Augerot, X., McHugh, P.A., and Bugaev, V.F. 2012. Global assessment of extinction risk to populations of Sockeye salmon Oncorhynchus nerka. PLoS One **7**(4). doi:10.1371/journal.pone.0034065.

Roni, P., Anders, P.J., Beechie, T.J., and Kaplowe, D.J. 2018. Review of Tools for Identifying , Planning , and Implementing Habitat Restoration for Paci fi c Salmon and Steelhead. (Noaa 2015): 355–376. doi:10.1002/nafm.10035.

Schwartz, J.S. 2016. Use of ecohydraulic-based mesohabitat classification and fish species traits for stream restoration design. Water (Switzerland) **8**(11): 1–33. doi:10.3390/w8110520.

Tonina, D., McKean, J.A., Benjankar, R.M., Wright, W., Goode, J.R., Chen, Q., Reeder, W.J., Carmichael, R.A., and Edmondson, M.R. 2018. Mapping river bathymetries: evaluating topobathymetric LiDAR survey. Earth Surf. Process. Landforms. doi:10.1002/esp.4513.

Wall, C.E., Bouwes, N., Wheaton, J.M., Saunders, W.C., and Bennett, S.N. 2016. Net rate of energy intake predicts reach-level steelhead (*Oncorhynchus mykiss*) densities in diverse basins from a large monitoring program. Can. J. Fish. Aquat. Sci. **73**(7): 1081–1091. doi:10.1139/cjfas-2015-0290.

Walters, A.W., Bartz, K.K., and Mcclure, M.M. 2013. Interactive Effects of Water Diversion and Climate Change for Juvenile Chinook Salmon in the Lemhi River Basin (U.S.A.). Conserv.

Biol. **27**(6): 1179–1189. doi:10.1111/cobi.12170.

Weber, N., Bouwes, N., Jordan, C.E., and Jonsson, B. 2014. Estimation of salmonid habitat growth potential through measurements of invertebrate food abundance and temperature. Can. J. Fish. Aquat. Sci. **71**(8): 1158–1170. doi:10.1139/cjfas-2013-0390.

Wheaton, J.M., Bouwes, N., Mchugh, P., Saunders, C., Bangen, S., Bailey, P., Nahorniak, M., Wall, E., and Jordan, C. 2018. Upscaling site-scale ecohydraulic models to inform salmonid population-level life cycle modeling and restoration actions – Lessons from the Columbia River Basin. Earth Surf. Process. Landforms **43**(1): 21–44. doi:10.1002/esp.4137.

Wilzbach, M.A., and Hall, J.D. 1985. Prey availability and foraging behavior of cutthroat trout in an open and forested section of stream. SIL Proceedings, 1922-2010 **22**(4): 2516–2522. doi:10.1080/03680770.1983.11897715.

Wohl, E., Lane, S.N., and Wilcox, A.C. 2015. The science and practice of river restoration. Water Resour. Res. **51**(8): 5974–5997. doi:10.1002/2014WR016874.

Woodward, G., Perkins, D.M., and Brown, L.E. 2010. Climate change and freshwater ecosystems: Impacts across multiple levels of organization. Philos. Trans. R. Soc. B Biol. Sci. **365**(1549): 2093–2106. doi:10.1098/rstb.2010.0055.

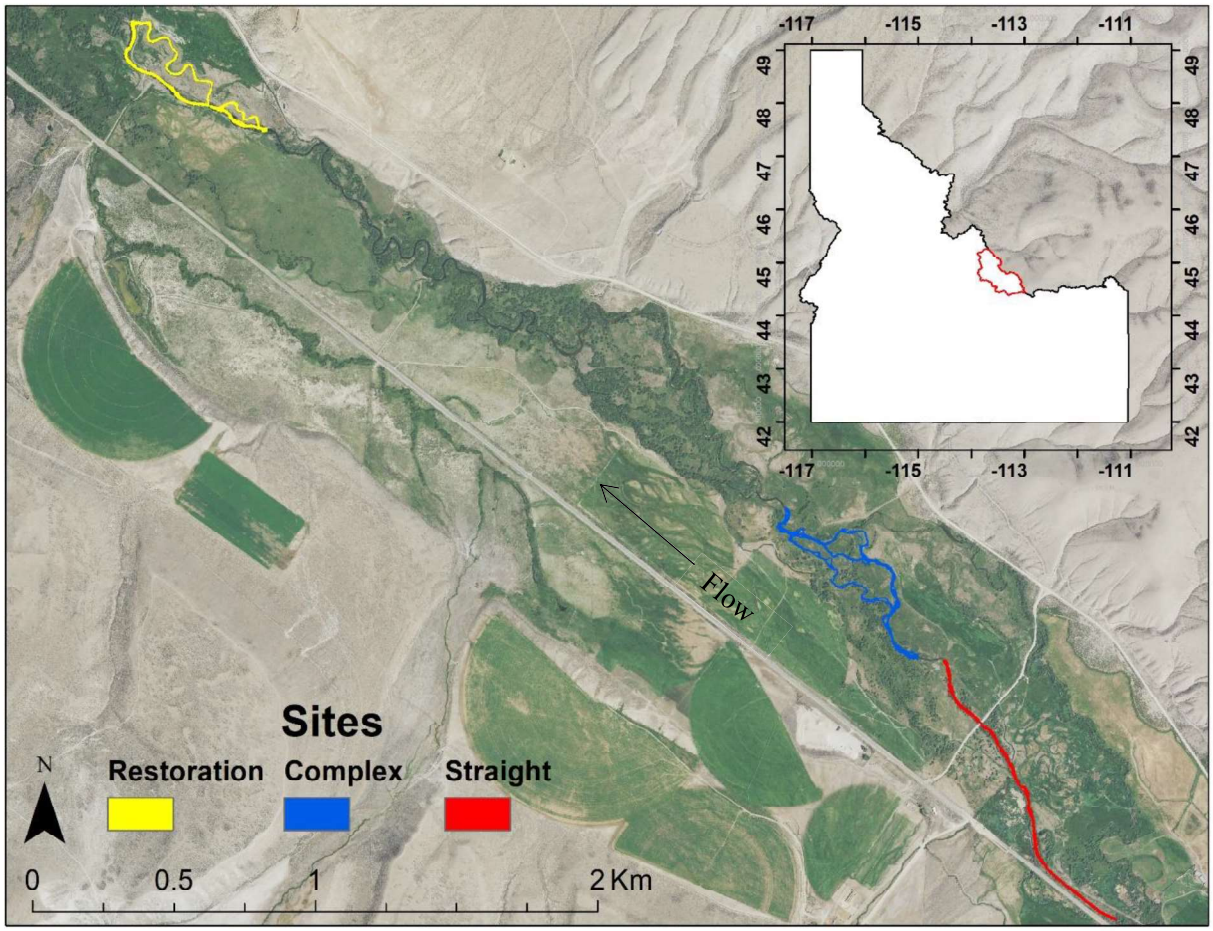

Figure 2-1. Map of the Lemhi watershed and spatial locations of each modeled reach; Complex, Restoration, and Straight. The inset shows the location of the Lemhi drainage within the state of Idaho, USA. The map is displayed over imagery from the National Agriculture Imagery Program, coordinates are in GCS North American 1983.

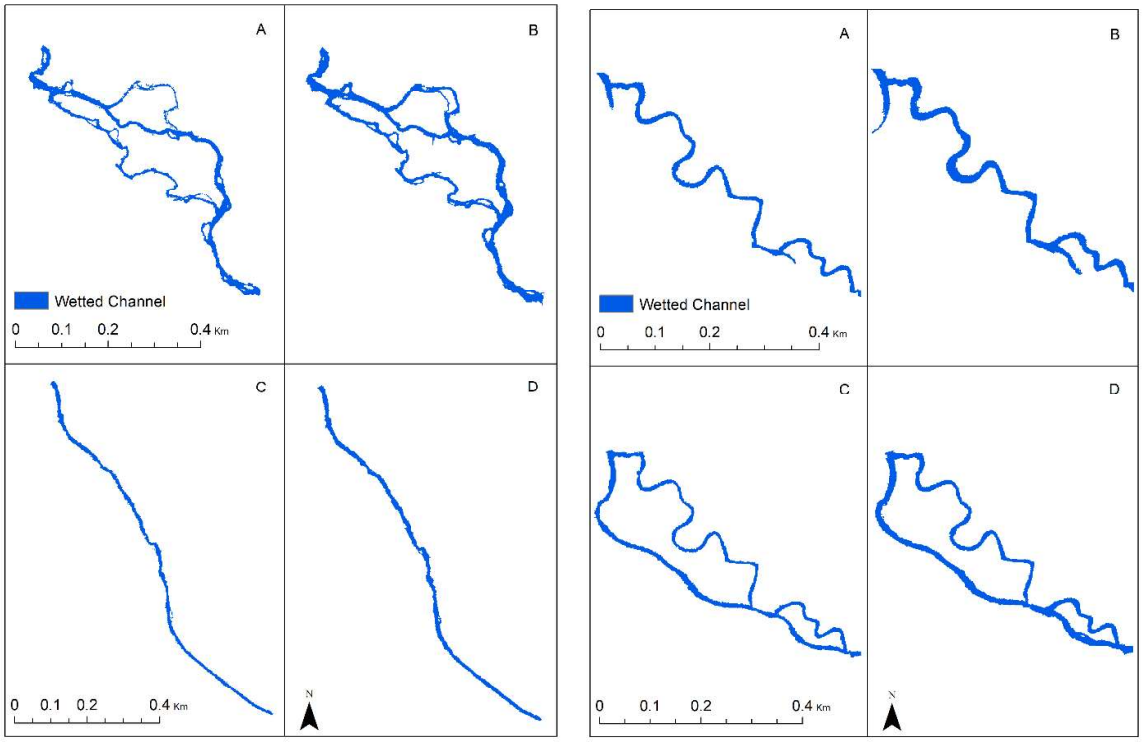

Figure 2-2. Maps of the wetted area of each modeled scenario/reach. A) Fully diverted Complex; B)Fully undiverted Complex; C) Fully diverted Straight; D) Undiverted Straight; E) Fully diverted Restoration Closed; F) Undiverted Restoration Closed; G) Fully diverted Restoration Open; H) Undiverted Restoration Open.

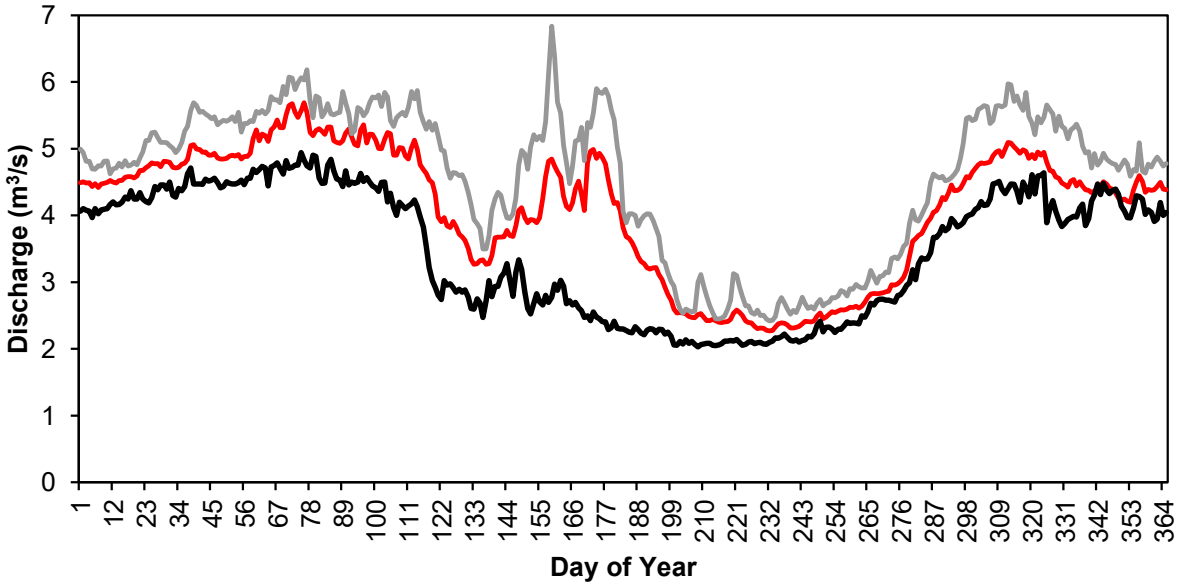

Figure 2-3. Daily average discharge (solid red line), along with its 75th percentile (gray line) and 25th percentile (black line) calculated from all available discharge measurements at the Lemhi at Cottom Lane Idaho Department of Water Resources gauging station just upstream of the study reaches.

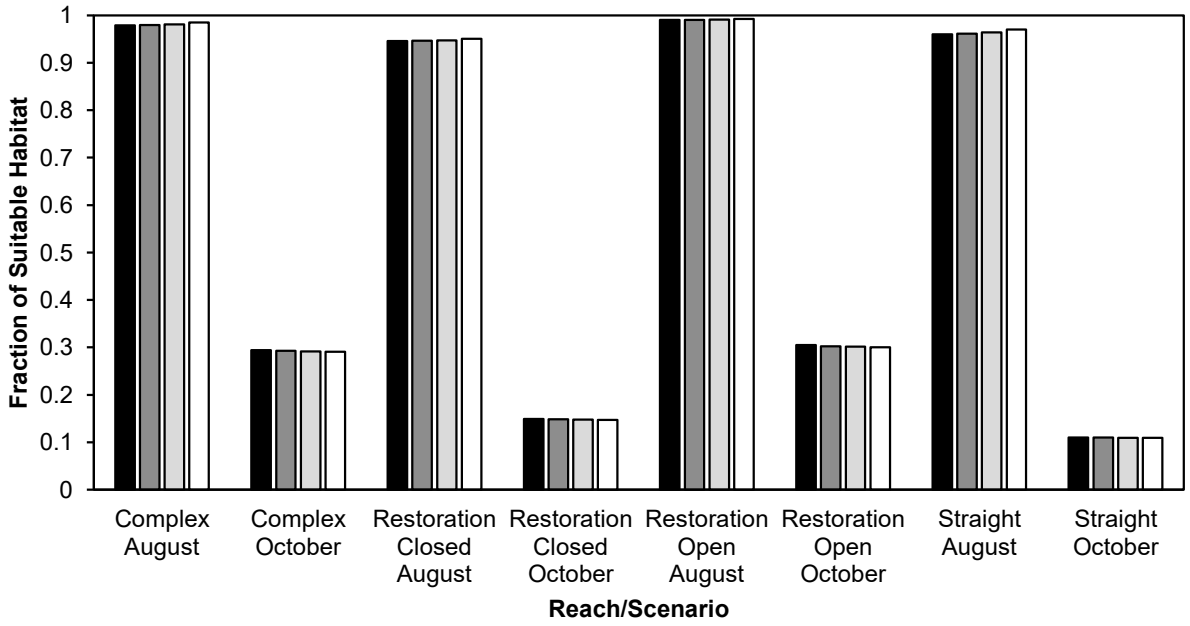

Figure 2-4. Calculated fraction of suitable habitat, defined with modeled NEI values meeting or exceeding the required maintenance ration for a given fork length, drift abundance, and temperature. Results are grouped by reach/flow scenario and colored by modeled fork length of 65, 75, 88, and 102 mm, from left to right and dark to light gray, respectively.

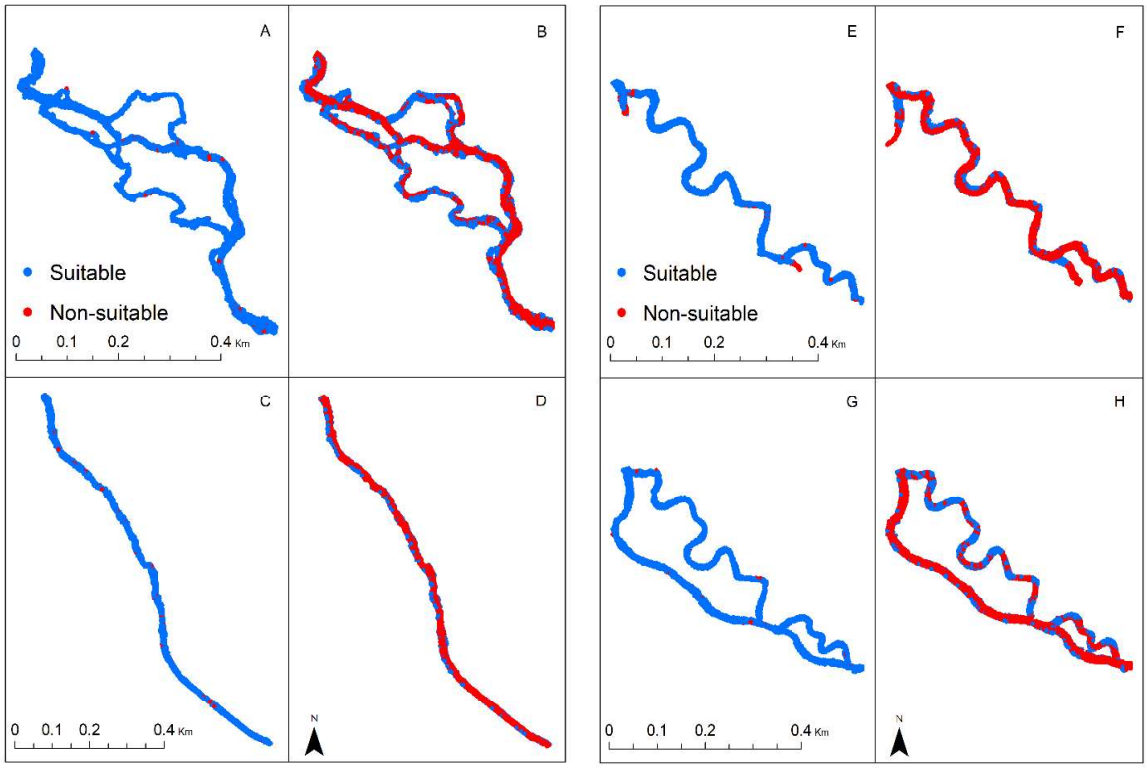

Figure 2-5. Spatially distributed results of all modeled feeding locations that either met or exceeded the calculated maintenance ration (AE ≥ 1) for the corresponding temperature and 50th percentile fork length of measured Lemhi River Chinook Salmon. Displaying all modeled reaches: A) Fully diverted Complex; B) Fully undiverted Complex; C) Fully diverted Straight; D) Undiverted Straight; E) Fully diverted Restoration Closed; F) Undiverted Restoration Closed; G) Fully diverted Restoration Open; H) Undiverted Restoration Open.

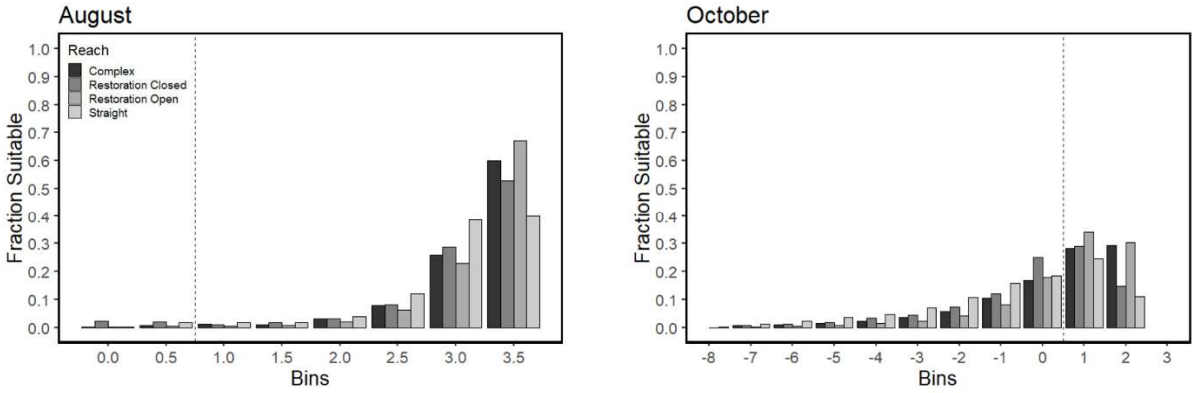

Figure 2-6. Histograms of AE, the ratio of NEI to maintenance ration, for both August and October modeled scenarios. The y-axis displays the fraction of habitat area that falls within each bin of AE. The bars are colored by the corresponding reach for the 50th percentile fork length. The dotted line marks a bin value of 1 or greater, which indicate feeding stations have met or exceeded the calculated maintenance ration.

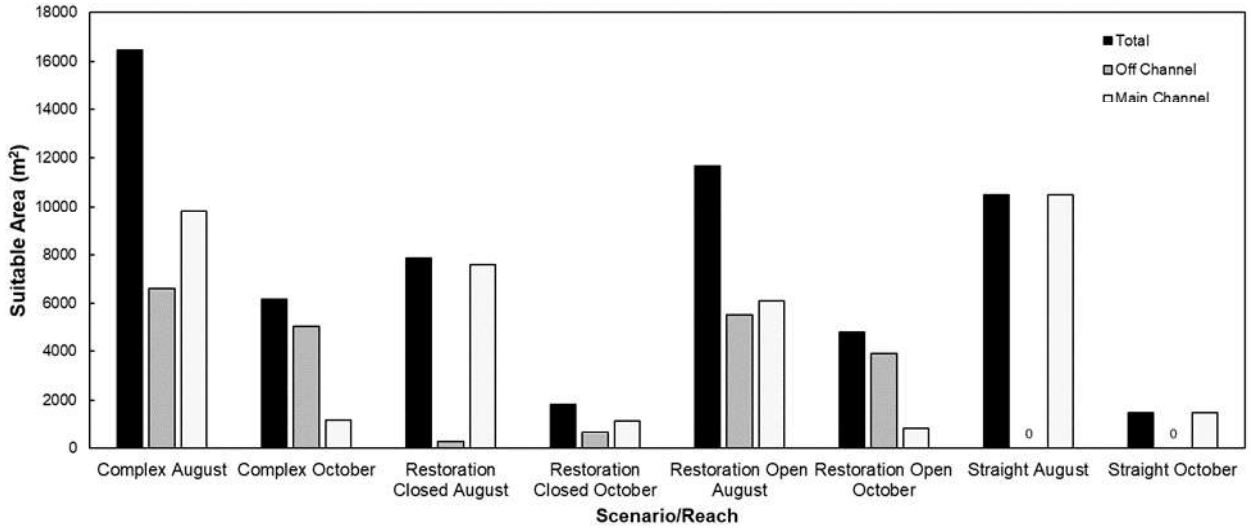

Figure 2-7. Total amount of suitable habitat (AE ≥ 1) for the entire reach, its main channel, and off-channel areas for the 50th percentile fork lengths of Lemhi River juvenile Chinook.

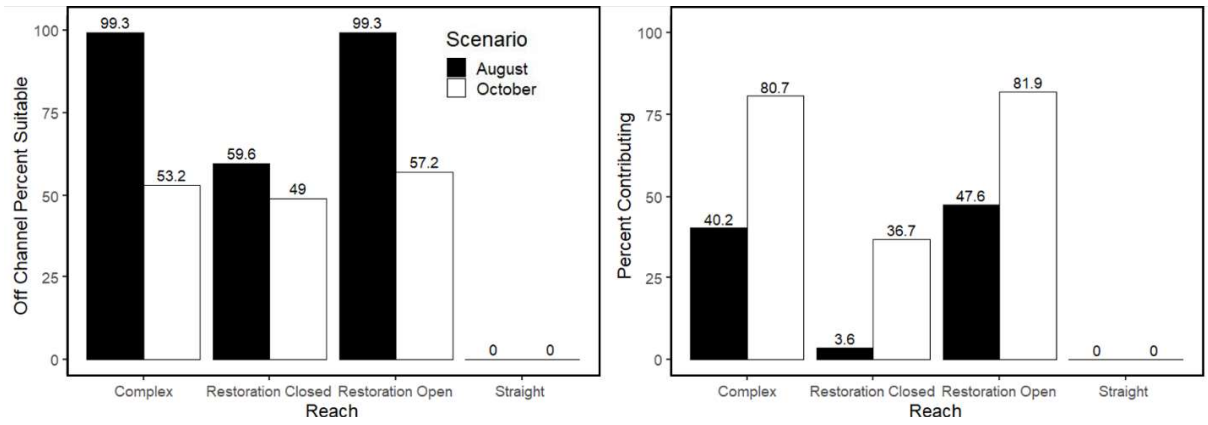

Figure 2-8. Percent of off-channel habitat with AE ≥ 1 (left graph) and percent of off-channel contribution to the total suitable area of each individual study reach and scenario (right graph).

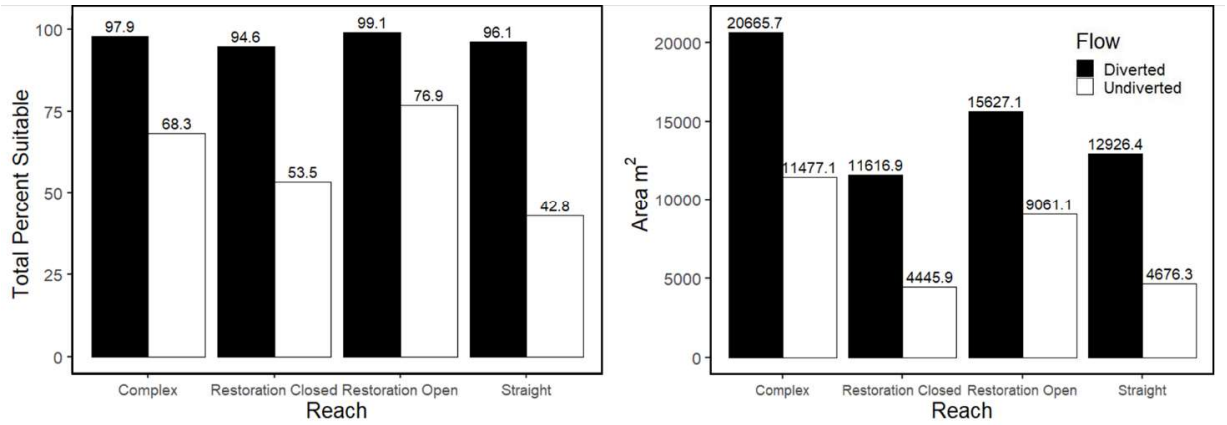

Figure 2-9. Total available suitable habitat for the late August alternative flow scenario (all other variables held constant) expressed in percent of total suitable habitat (left graph) and in area (m^2) for the diverted and undiverted flows.

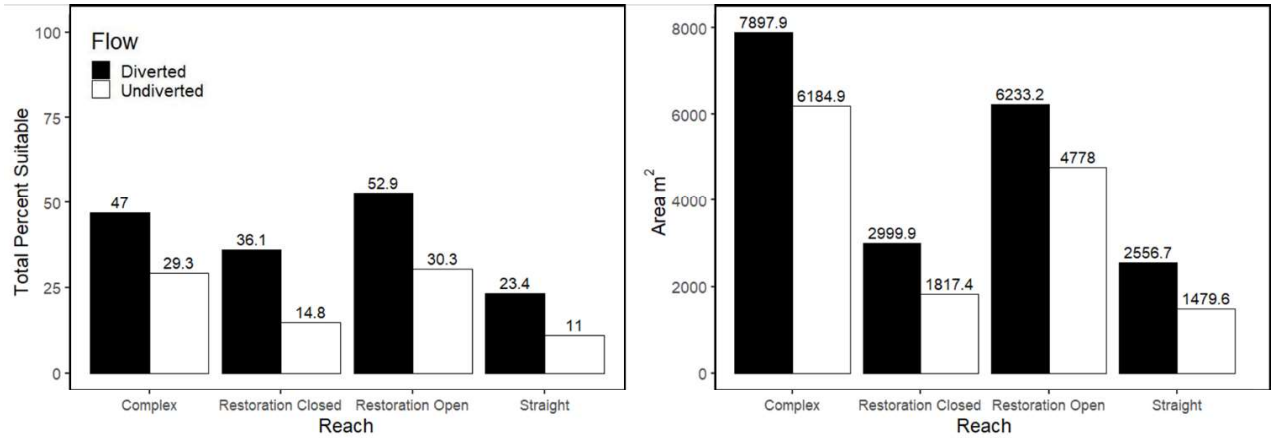

Figure 2-10. Total available suitable area for late October alternative flow scenario expressed in percent (left graph) and in area (m^2) (right graph) for diverted and undiverted flow.